COO-5100-3

GAMMA-RAY ENERGY RESPONSE OF ^{7}LiF AND CaF_2:Mn TLDS

Annual Report

G. G. Simons

Kansas State University
Department of Nuclear Engineering
Manhattan, Kansas

November 1979

Prepared for

The U.S. Department of Energy

Under Contract No. ET-78-S-02-5100

DISCLAIMER

Gamma-Ray Energy Response of ^{7}LiF and CaF_2:Mn TLDs

Annual Report

G. G. Simons
Kansas State University
Department of Nuclear Engineering
Manhattan, Kansas

November 1979

Prepared for

The U.S. Department of Energy

Under Contract No. ET-78-S-02-5100

TABLE OF CONTENTS

TABLE OF CONTENTS (cont'd)

LIST OF FIGURES

LIST OF FIGURES (cont'd)

LIST OF TABLES

LIST OF TABLES (cont'd)

Gamma-Ray Energy Response of ^{7}LiF and CaF_2:Mn TLDs

G. G. Simons

Abstract

The gamma-ray energy responses of encapsulated ^{7}LiF and CaF_2:Mn thermoluminescent dosimeters were measured and compared to calculated values. This study was performed in order to improve the accuracy of gamma-ray heating measurements made in polyenergetic gamma-ray fields such as Argonne National Laboratory's Zero Power Reactors. Comparisons between calculations and experiments are reported for a gamma-ray energy range of 0.122 to 1.33 MeV and encasement media with a range of atomic numbers from 13 to 82.

I. Introduction

Thermoluminescent dosimeters are receiving international attention for measuring the gamma-ray energy deposition in various regions of critical assemblies such as the Argonne National Laboratory (ANL) Zero Power Reactors (ZPRs). This interest was largely generated by the successful demonstration of the technique by scientists within the ANL Applied Physics (AP) Divison [1-4]. Intercomparison of the results obtainable, and procedures used, by the experts in the field provides the opportunity for exchanging information between the United States and foreign nations. Moreover, careful examination of the procedures used will enhance the understanding of the subject. Data reported in this report may allow measurement of more accurate gamma-ray heating data through identification and resolution of systematic errors.

One area of immediate interest in the interpretation of TLD excitation was the subject of this study -- the gamma-ray energy response of encapsulated TLDs. A method devised by Burlin [5] served as the basis for the TLD Energy Response Code (TERC) computer code written for the analyses of gamma-ray heating experiments at ANL [6]. The latest version, TERC/III, was used in this investigation to calculate the energy response of encased TLDs. These calculations were performed as a function of the TLD and encasement materials, TLD size, and gamma-ray energy.

II. Theory

The solid state ionization theory used to calculate the dose ratio factor

$$f(T_\gamma) = E_D/E_M$$

where E_D is the predicted absorbed dose in the dosimeter and E_M is the predicted absorbed dose in the medium surrounding the dosimeter is presented in Ref. 7. Input data used to calculate $f(T_\gamma)$, using the TERC/III computer code, are discussed and tabulated in this section.

A. Average Attenuation Factor

The size of the TLD was accounted for using the average attenuation factor $d(T_\gamma,x)$ where

$$d(T_\gamma,x) \equiv d = \frac{1-e^{-\beta(T_\gamma)g}}{\beta(T_\gamma)\ g} \quad . \tag{1}$$

Values for $\beta(T_\gamma)$, the electron attenuation coefficient were calculated by assigning a 1% transmission to the range $R(T_\gamma)$ so

$$\beta(T_\gamma) = \frac{-\ln\ 0.01}{R(T_\gamma)} \tag{2}$$

where

$$R(T_\gamma) = 0.412\ T_\gamma^n \quad \text{for} \quad 0.01 \leq T_\gamma \leq 3\ \text{MeV}$$

$$n = 1.265 - 0.0954\ \ln\ T_\gamma$$

and T_γ is defined as the maximum electron energy corresponding to the energy of the primary gamma ray.

For a convex TLD and an isotropic electron flux, the mean chord length, g, is given by

$$g = 4V\rho/S\ (g/cm^2) \tag{3}$$

where

V = volume of the TLD (cm^3)

S = surface area of the TLD (cm^2)

ρ = density of the TLD (g/cm^3)

The two parameters input to TERC/III were ρ and g. These are listed in Table I for 1x1x6 mm ^7LiF and CaF_2 TLDs.

B. Collision Mass Stopping Powers

Collision mass stopping powers (MSPs) for the encasement materials and the TLDs can either be read-in as input data or calculated internally. Equations used to calculate these quantities were derived from the work reported in Ref. 8.

Input data required to calculate MSPs were Z/A, I, and the density effect parameters. These data are listed in Tables I and II for the TLD and the encasement materials respectively.

To evaluate the MSPs calculated using TERC/III and those reported by other investigators, an intercomparison was completed. Table III presents the results for LiF reported by Berger and Seltzer (8) and those calculated with TERC/III. A comparison for two independent MSP calculations are shown in Table IV for CaF_2. Absolute values and the resulting ratio's for each type of encasement material, which were reported in Ref. 8, are shown in Tables V-IX. In addition, values of TERC/III calculated MSPs for materials not calculated by Berger and Seltzer of interest in this research, are listed in Table X.

C. Mass Energy Absorption Coefficients

Mass energy absorptions (MEA) coefficients were also input parameters. MEA coefficients used for ^7LiF and CaF_2 are listed in Tables XI and XII. Each set of coefficients are also compared to values used by other investigators. A systematic difference did not exit between these

data since the average ratio of the data was 1.0017 ± 0.0158 for LiF and 0.9958 ± 0.0181 for CaF_2. However on an energy by energy basis differences exceed 3% for both types of TLDs. MEA coefficients for the encasement materials, taken from Ref. 9, are tabulated in Tables XIII and XIV.

It is common to consider MEA coefficients as having errors of the order of 10%. Therefore, in any study which depends upon MEA coefficients, it is important to specify the exact data used. Otherwise precise intercomparison studies or reproduction of earlier work is impossible.

III. TERC/III Calculations

Dose ratio factors $f(T_\gamma)$ were calculated for all of the sleeve materials and gamma-ray energies investigated. Tables XIII and XIV list the TERC/III calculated $f(T_\gamma)$ values.

IV. Experimental Equipment and Devices

Experimental equipment, within the K-State Nuclear Engineering Department's Instrumentation Laboratory, which was available for this project are described in this section. The TLD Analyzer was purchased using K-State funds provided by the Department of Nuclear Engineering. The TLDs, gamma-ray sources, and the irradiation device were obtained using project funds.

A. Data Acquisition Equipment

TLDs were read using a Model 2000 Thermoluminescence Analyzer purchased from the Harshaw Chemical Company. As shown in Fig. 1 this instrument contained two units (1) a model 2000-A TL Detector and a (2) Model 2000-B Automatic Integrating Picoammeter.

Glow curves (PM tube current versus time or temperature) and temperature profiles were measured with an X-Y recorder. This X-Y recorder

was used only when a permanent record was required. Normally, only the LED displayed total charge from the PM tube was recorded during TLD heating. This was the desired quantity used to relate the instrument output to the gamma ray induced excitation within the TLD. The temperature profile and a few glow curves were measured with the X-Y recorder during setup of the TLD analyzer.

B. Annealing and Handling Equipment

Two ovens and a constant temperature enclosure were available for TLD annealing. A high temperature (30 to 1200°C) Thermolyne Type 10500 furnace containing solid-state temperature controllers was used to pre-anneal the TLDs at 400°C. The second oven, used for pre-annealing of LiF at 100°C, was a Thelco Precision Oven Model 16 having a temperature range of 0 to 200°C. A metal cabinet drawer below the ovens served as a draft free TLD cooling chamber.

The individuality of each TLD was retained by placing them into a pyrex petri dish. Copper and aluminum have a high thermal conductivity but a black oxide layer was formed when heated at 400°C. This oxide would have contaminated the surface of the TLD rods.

Special tweezers were required to handle the small TLD rods. They consisted of small metal tweezers whose ends had been covered with heat shrinkable tubing. Both metal and plastic tweezers are inferior to the "shrink-fit" type since they are prone to scratching and crushing the delicate TLDs.

C. TLDs

One thousand each of two types of TLDs were purchased from the Harshaw Chemical Company. One type was high sensitivity lithium fluoride

which were 6-mm-long, 1-mm-square solid rods enriched to 99.993% ^{7}Li (TL-700). The other type was CaF_2:Mn (TL-400) of the same size.

D. Gamma-ray Sources

The six gamma-ray sources, listed in Table XV, were purchased from Isotope Products Laboratories. Each source was individually encapsulated in a special capsule as shown in Fig. 2. Source material was made as small as possible in order to approximate a point source. The capsule was designed to provide for radial symmetry and minimum attenuation of the primary gamma rays by the encapsulation material.

F. Encasement Materials

Encasement materials used to experimentally evaluate relative values of f for this study are listed in Table XVI. As shown in this table, each sleeve had a desired nominal thickness of 0.7 g/cm^2.

V. Experimental Procedures

Establishing of a good experimental procedure was critical in order to measure high precision data. A procedure which had proven successful in previous TLD research work was followed (7). This included using sensitivity selection. Moreover, a systematic procedure was adhered to for 1) handling, 2) pre- and post-annealing, 3) encapsulation, 4) calibration, 5) exposure/wait/readout schedule, and 6) readout method and instrumentation. All CaF_2:Mn TLDs were also kept in a dark environment during and following irradiation to minimize systematic errors stemming from the troublesome light induced fading of CaF_2:Mn TLDs.

A. Readout Procedures

The operating procedure adopted for recording the TL from TLDs was the same as described in Ref. 10.

B. Annealing

Pre-irradiation annealing consisted of the following steps: (1) the TLDs were placed in a pyrex petri dish, then (2) placed in a 400°C oven for one hour, (3) cooled for ten minutes on an asbestos pad in a draft free drawer, (4) placed in a 100°C oven for two hours, and finally (5) cooled to room temperature in the manner specified in step (3). As mentioned in Section IV.B., TLDs were annealed in the pyrex dishes because of the tendency of most other materials to form an oxide when heated to high temperatures.

Post-irradiation annealing was not used. This would have involved handling the TLDs one additional time. Because of the difficulty of maintaining the individual identity of each TLD and the systematic errors induced by handling a TLD it was decided that maximum precision would be achieved if post-irradiation annealing was omitted. Instead, 24 hours between the end of the irradiation and the start of the analysis of each TLD was chosen are the best procedure.

C. Calibration

Even though it was not necessary to obtain absolute absorbed dose values in this research, a limited scope calibration was performed for each type of TLD. The results are shown in Figs. 3 and 4. These two experiments were performed to evaluate the low dose response characteristics of the TLD analyzer.

D. Encasement

In general, in order to interpret the readout of a TLD, it is necessary to specify the medium surrounding the TLD. If the surrounding medium is properly characterized, and if the energy response of the encapsulated TLD and the gamma-ray spectrum are known, then the TLD readout can be converted to the dose in the desired material.

The solid state ionization theory used in this study required that the thickness of the encasement material was great enough to ensure electron equilibrium in the material. Electron equilibrium was established at the site of the TLD provided that the same energy was removed from as entered the TLD. This meant that for every electron leaving the TLD, another electron of about the same energy entered the TLD. Thus consideration was given to equilibrium relative to the electrons produced in the medium by the radiation field whose dose was to be measured.

In practice, an acceptable prescription does not exist for choosing the thickness to be used for all applications. However, it is known that if the surrounding medium is too thin, then the dose measured at the TLD will be less than for the case when electron equilibrium existed. Conversely, if the wall is arbitrarily choosen and is too thick, serious attenuation of the primary radiation incident upon the dosimeter will occur and the resulting TLD derived dose will also be too low.

In this research, essentially only one sleeve thickness was investigated. This thickness -- nominally 0.7 g/cm^2, was the same as previously chosen for measuring gamma-ray heating in cores and blankets of the Zero Power Plutonium Reactor operated by ANL[4]. During this ANL study, emphasis was placed upon measuring gamma-ray heating in stainless steel. However, data reported in this research can be used to extend the application of TLDs encased in nominally the same thickness sleeve but surrounded by materials having a range of atomic numbers.

E. Sensitivity Selection

Intra-batch sensitivity selection was used to improve the precision of the energy response data (7). This involved grouping TLDs according to their relative sensitivity. Sensitivity was measured by irradiating groups of 200 new TLDs at one time (a typical result

is shown in Fig. 6 . The resulting nc charge obtained from each TLD was used as input data to the Sort and Dose (SAD) computer code. Precision subsets were obtained, upon processing these data, in terms of TLD identification number and relative sensitivity for each TLD whose nc value was within $\pm$ 6% of the group mean. TLDs which had sensitivities outside this limit were not used in subsequent measurements.

F. Irradiations of Encased TLDs

TLDs from a given precision subset were placed inside the sleeve materials and irradiated at concentric positions on the styrofoam (Fig. 5) holder. Separate irradiations were performed, with each gamma-ray source, using all eight types of encasements. Moreover, to reduce the error associated with each reported value, ten sleeves of each type were used during each irradiation.

VI. Methods of Comparison

Results of this investigation are presented as calculated C/E values and in terms of the number of source decays. The C/E values were obtained as follows. The TERC/III calculated dose ratio for the dosimeter (E_{Di}), relative to the encasement material (E_{Mi}), was defined as

$$f_i(T_\gamma) = \frac{E_{Di}}{E_{Mi}} \tag{4}$$

where i corresponds to the type of encasement material. The equation for the total absorbed dose in a material of type i, exposed to a gamma-ray source emitting photons having a single energy, T_γ, is

$$E_{Mi} = \frac{T_\gamma St}{4\pi r^2} \left[\frac{\mu_{en}\ (T_\gamma)}{\rho}\right]_{Mi} \frac{MeV}{g} \tag{5}$$

where S (γ/sec) is the gamma-ray intensity, t (sec) is the exposure time and r (cm) is the source to dosimeter distance. Substituting Eq. (4) into Eq. (5) and rearranging terms gives

$$\frac{T_\gamma St}{4\pi r^2} = \frac{E_{Di}/f_i(T_\gamma)}{\left(\frac{\mu_{en}(T_\gamma)}{\rho}\right)_{Mi}} \tag{6}$$

From Eq. (6), an expression for the calculated dose in the TLD can be written as

$$E_{Di} = K \left(\frac{\mu_{en}(T_\gamma)}{\rho}\right)_{Mi} f_i(T_\gamma) \tag{7}$$

where K is a constant equal to the left hand side of Eq. (6). By choosing a reference sleeve material, denoted by the subscript j, an equation for the calculated dose which was independent of K was defined as

$$C = \frac{E_{Di}^{calc}}{E_{Dj}^{calc}} = \frac{\left(\frac{\mu_{en}(T_\gamma)}{\rho}\right)_{Mi} f_i(T_\gamma)}{\left(\frac{\mu_{en}(T_\gamma)}{\rho}\right)_{Mj} f_j(T_\gamma)} \tag{8}$$

The corresponding experimental dose was

$$E = \frac{E_{Di}^{exp}}{E_{Dj}^{exp}} \quad . \tag{9}$$

Significant attenuation, of the low energy gamma-ray, occurred in the high Z encasement materials. An approximate correction of the form

$$C(T_\gamma, x) = \exp\left(\frac{\mu_{en}(T_\gamma)x}{\rho}\right) \tag{10}$$

where $\mu_{en}(T_\gamma)/\rho$ is the mass energy absorption coefficient of the sleeve material, and x is the sleeve thickness, could be applied to the C/E values. Reported data were not corrected for sleeve attenuation since a more detailed investigation of sleeve thickness is being performed.

The expression used to calculate the relative number of source decays, S, derived in Ref. 7, was

$$S = \left[\frac{D\,K\,4\pi r^2}{\sum_i T_i\,W_i\,\frac{\mu_i}{\rho}\,f_i}\right]_M \qquad (11)$$

where

D = value proportional to the measured dose in the TLD

K = constant

r = distance from the source to the TLD

T_i = energy of gamma ray i

W_i = probability of release during decay

μ_i/ρ = mass energy absorption for gamma ray i

f_i = dose ratio for gamma ray i

For a given gamma-ray source, S would be a constant for all encasement materials, M, because the irradiation conditions were the same. The degree of constancy of S as a function of the atomic number of the sleeve material formed the basis for intercomparing the measured and calculated energy response of the encapsulated TLDs.

VII. Results

A. Experimental Data

The TL emitted from encapsulated CaF_2:Mn and high sensitivity ^7LiF TLDs was measured following irradiation with gamma rays. A range of atomic numbers from 13 to 82, for the media surrounding each type of TLD, was investigated using the encasement materials described in Section IV.-F. Gamma-ray energies studied were 0.122, 0.136; 0.145, 0.279, 0.393, 0.662, and 1.173, 1.333 MeV. Characteristics of the gamma-ray sources were presented in Section IV-D. Since this study was based upon the relative response of encapsulated TLDs, each reported value was normalized to the appropriate TL for an iron encased TLD.

Each dosimeter, used in this study, consisted of a cylindrical sleeve which housed a 1 x 1 x 6 mm TLD. These dosimeters were nominally 3.2 mm in Dia. x 12.7 mm long. In order to reduce the standard deviation associated with each final energy response result, ten similar TLDs were individually encased in identical sleeve materials. These sets of dosimeters, containing eight encasement materials and one type of TLD, were simultaneously irradiated using a single gamma-ray source. This procedure was discussed in Section V-F. Additional information, pertaining to the experimental procedure, is contained in Section V. Raw TL data, recorded from each TLD, were processed to obtain the average TL per group of ten TLDs. These group averaged values were then normalized relative to the mean value of the iron encased TLD. the experimental results are listed in Tables XVII and XVIII

for ^{7}LiF and CaF_2:Mn TLDs processed using this direct procedure. These data represent the results obtained using groups of pre-selected TLDs. Their relative TL, measured during the individual sensitivity evaluation, was within ±6% of the average TL for the original group of 200 new TLDs.

An alternate data reduction technique, based upon the sensitivity of the individual TLDs, was also used to process these data. This involved using the sensitivity factor measured during the intra-batch sensitivity selection experiments (see Section V-E.). A correction factor was applied to each TL value recorded following irradiation of the encased TLDs which had different individual sensitivities to gamma radiation. Within the errors of the sensitivity data, the sensitivity of all the TLDs were forced to be equal to the average value of the corresponding precision subset. After applying the sensitivity correction, the data were averaged and normalized to the iron encasement result. Relative energy response results are listed in Tables XIX and XX for the two types of TLDs corrected for individual sensitivity.

B. Comparisons Between Experiment and Calculation

Comparisons between the calculated (C) energy responses of an encapsulated TLDs and the measured (E) responses were completed for all combinations of TLD type, gamma-ray energy, and encasement material. Two approaches were used to accomplish this. The first, very amenable to providing meaningful tabular results, was based upon using Eq. 8 to calculate the response and comparing these C values to the corresponding experimental dose (E) from Eq. 9. Conversely, the source decay developement (see Eq. 11) allowed the results to be represented graphically. Tabular values are, obviously, of more value to future investi-

gators who wish to either use these results directly or compare them to other similar studies. The figures, resulting from the graphical representation, will allow the casual observer the opportunity to rapidly scan these results and note the trends in the source decay model.

Direct C/E calculations were obtained using Eqs. 8 and 9. Calculated values of C were based upon the dose ratio and mass energy absorption coefficients generated using the TERC/III code. Specific numbers are listed in Tables XIII and XIV for both types of TLDs investigated. Iron sleeves were chosen as the reference in order to provide C results directly comparable to the normalized experimental data. Common C quantities for each type of sleeve material, gamma-ray energy and TLD type were used to calculate the C/E results listed in Tables XXI-XXIV. Different E values were used since they were extracted from the previously discussed experimental results for encased TLDs with and without correction for individual sensitivity.

The relative number of source decays (S) were calculated using the expression given by Eq. 11. Calculations were made for each combination of TLD, sleeve material, and gamma-ray energy. D values were picked from the sensitivity corrected TLD TL data. Mass energy absorption coefficient values were the same as used for the C/E determination. This study was, however, more comprehensive than the C/E one because an intercomparison was made between the experimentally derived energy response and three theoretical models. The C/E results were based upon solid state theory only. Source decay intercomparisons were made using the following models--1. small cavity theory, where in the limit, the cavity size is effectively zero, 2. solid state theory, the model proposed for TLD investigations, and 3. large cavity,

where in the limit the cavity is effectively infinite. Dose ratios for all three models, routinely calculated in the TERC/III code, were substituted for f_i in Eq. 11. The results are shown in Figs. 7-18 for the three models--small (S_s), solid state (S_{ss}), and large (S_L).

VIII. Conclusions

Benchmark data were obtained which can, in particular, be used directly to characterize the energy response of encapsulated ^{7}LiF and CaF_2:Mn TLDs. In general, these data are suitable for evaluating ionization theory models. Assumptions are an inherent part of any model. Ionization theory is no exception. Several approximations were made in developing the theory behind the TERC/III code (6). For example, it was assumed that bremsstrahlung and delta ray production could be ignored, that the volume averaged electron spectrum could be represented as a simple weighted sum of the distributions that are characteristic of the sleeve and dosimeter materials, and that electrons slow down continuously in these materials. C/E results offer a powerful means for deciding the range over which the results of a particular model are applicable. Even the most complex models are restricted in accuracy by the values of the input data used. Energy and atomic number limits must be established for each model before it can be used with confidence.

The results presented showed that consistent results were obtainable, using the experimental procedures outlined in Section V, for both types of TLDs. Adherence to prescribed procedures and sensitivity selection can be cited as the prime reasons for the small random errors. Intra-batch sensitivity selection allowed measurement of radiation doses to within nominally 2% for CaF_2:Mn and 3% for ^{7}LiF TLDs when 10 TLDs were used per configuration. This random error was reduced to about 1% when sensitivity corrections were applied to the individual TLDs.

C/E values varied depending upon the energy of the gamma rays and the atomic number of the sleeve material. They were nominally unity for two conditions--1. high energy gamma rays and all atomic numbers and 2. lower atomic numbers and all energy gamma rays. For the reverse combinations of energy and atomic number, signigicant deviations from unity were reported for both types of TLDs. It is hypothesized that the two main factors contributing to these findings were--1. systematic errors in the values used for the mass energy absorption coefficients and 2. attenuation of the gamma rays in the sleeve material surrounding the TLD. This latter factor would include both absorption and scatter of gamma rays.

Systematic errors in mass absorption coefficients would, in general, tend to cancel since dose ratios were used throughout this investigation. However, this cancelling effect would become less pronounced as the ratio of sleeve to iron atomic numbers increased. It was expected that these systematic errors would be minimized by using a consistent set of mass energy absorption coefficients. Naturally, a different set of coefficients would change the C/E values.

Correcting for sleeve attenuation, using Eq. 10, would improve the C/E comparisons. It would not, however, provide acceptable results for the lower energy and higher atomic number conditions.

Likewise, the solid state theory based relative number of source decay results predicted the response of encapsulated TLDs in the same manner as discussed above for the C/E intercomparisons. Neither the large cavity nor the small cavity theories were appropriate for the TLDs used in this study.

Additional investigations should concentrate on developing a prescription which can be used to account for the effect of sleeve thickness. This would complement the requirement for charged particle equilibrium.

References

1. G. S. Stanford and R. W. Johnson, "Determination of Gamma-Ray Heating in a Critical facility by Thermoluminescent Dosimetry," ANL-7373, Argonne National Laboratory (1968).

2. G. G. Simons, et al., "Gamma-Ray Dose Evaluations for the ZPR-3/ EBR-II Critical Assemblies," Trans. Am. Nucl. Soc., 13, 880 (1970).

3. G. G. Simons and A. P. Olsen, "Analysis and Measurements of Gamma-Ray Heating in the Demonstration Benchmark Plutonium-Fueled Critical Assembly," Nucl. Sci. Eng., 53, 176 (1974).

4. G. G. Simons and T. J. Yule, "Gamma-Ray Heating Measurements in Zero-Power Fast Reactors with Thermoluminescent Dosimeters," Nucl. Sci. Eng., 53, 162 (1974).

5. T. E. Burlin, "A General Theory of Cavity Ionization," Brit. J. Radiol., 39, 727, (1966).

6. G. G. Simons, "TERC/I --- TLD Energy Response Code," ANL-8010, Argonne National Laboratory, 436 (1975).

7. G. G. Simons and L. L. Emmons, "Evaluation of Gamma-Ray Response Calculations for ^{7}LiF TLDs," NIM, 160 79 (1979).

8. M. J. Berger and S. M. Seltzer, "Additional Stopping Power and Range Tables for Protons, Mesons, and Electrons," NASA SP-3036 (1965).

9. Ellery Storm and H. I. Israel, Photon Cross Sections from 1 keV to 100 MeV for Elements Z=1 to Z-100, Nucl. Data Tables, A7, 565 (1970).

10. G. G. Simons and T. S. Huntsman, "Evaluation of Thermoluminescent Dosimeters for Gamma Ray Dose Measurements in ZPPR," unpublished report (1971).

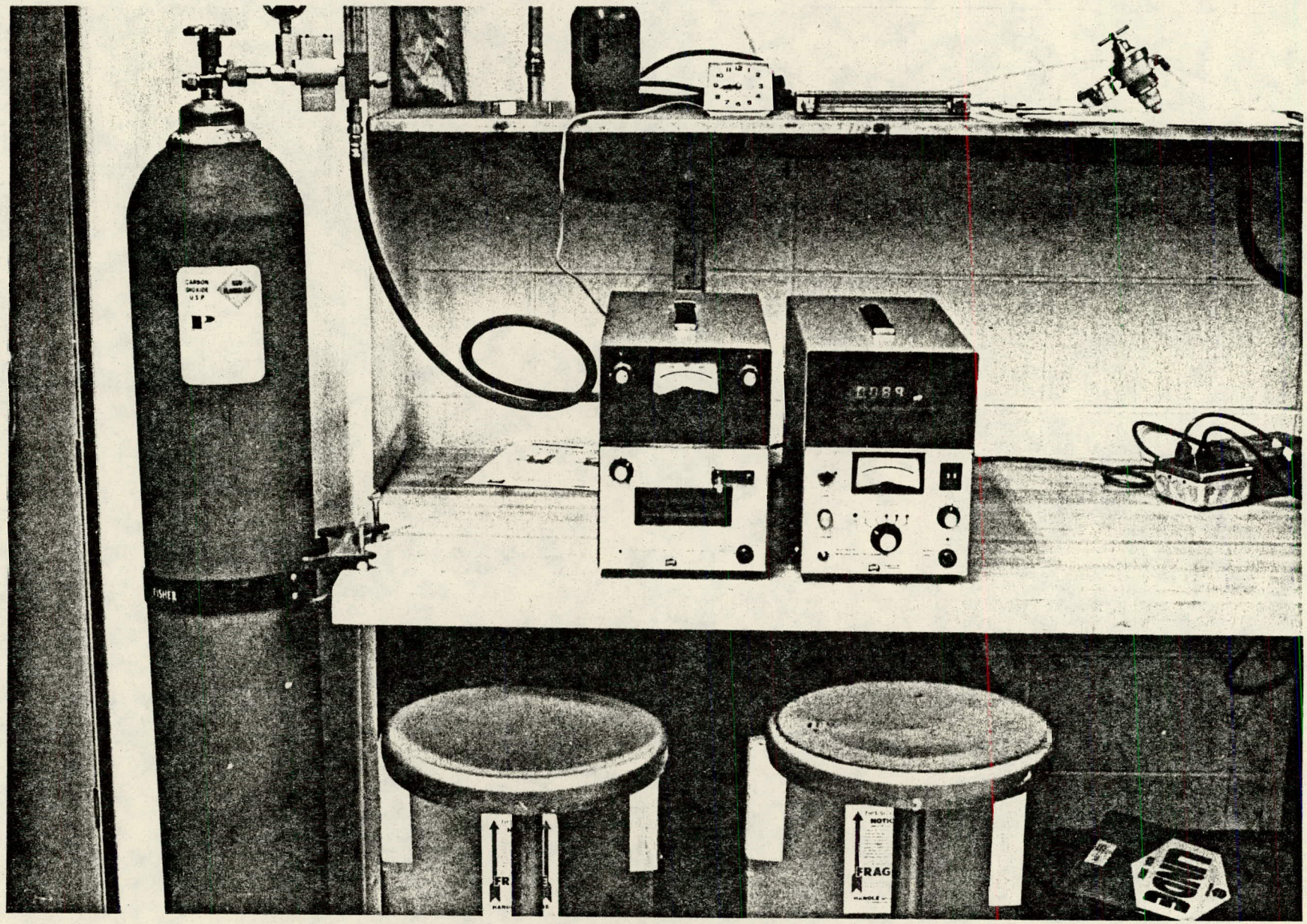

Fig. 1. Photograph of the Harshaw Model 2000 TLD Analyzer located in the Nuclear Engineering Department's Instrumentation Laboratory.

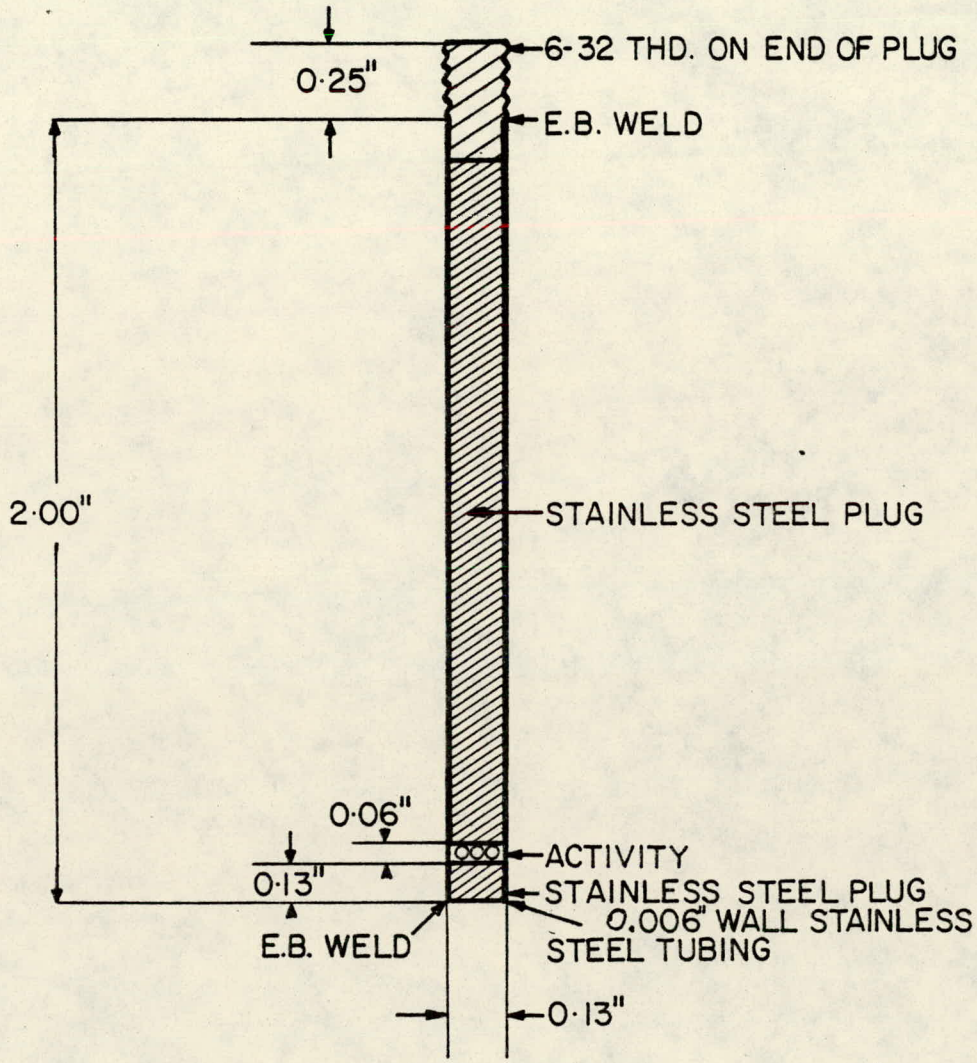

Fig. 2. Gamma-ray Source Capsule for the TLD Energy Response Study.

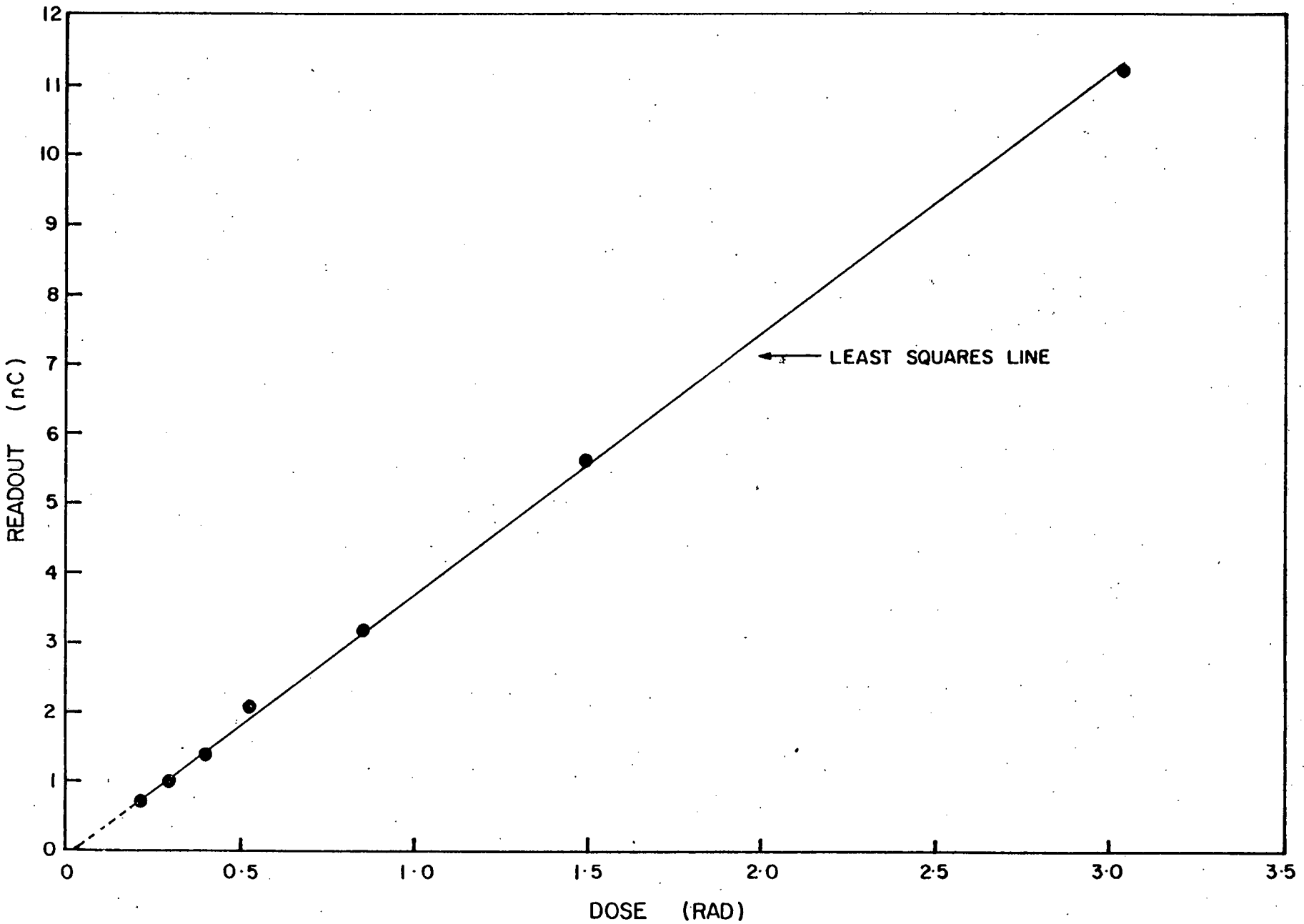

Fig. 3. Calibration Curve for 1x1x6 mm ^{7}LiF Thermoluminescent Dosimeters.

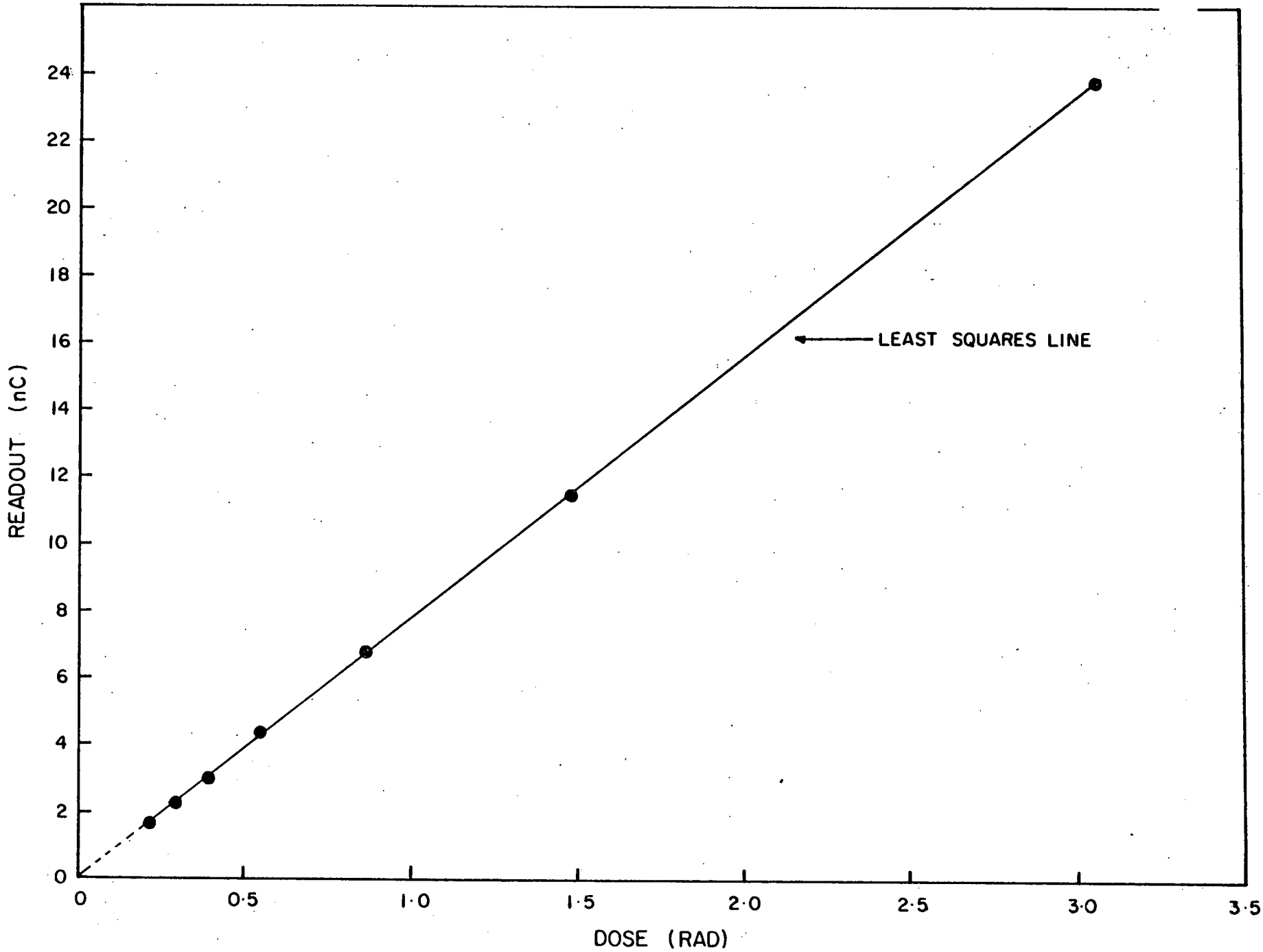

Fig. 4. Calibration Curve for 1x1x6 mm CaF_2:Mn Thermoluminescent Dosimeters.

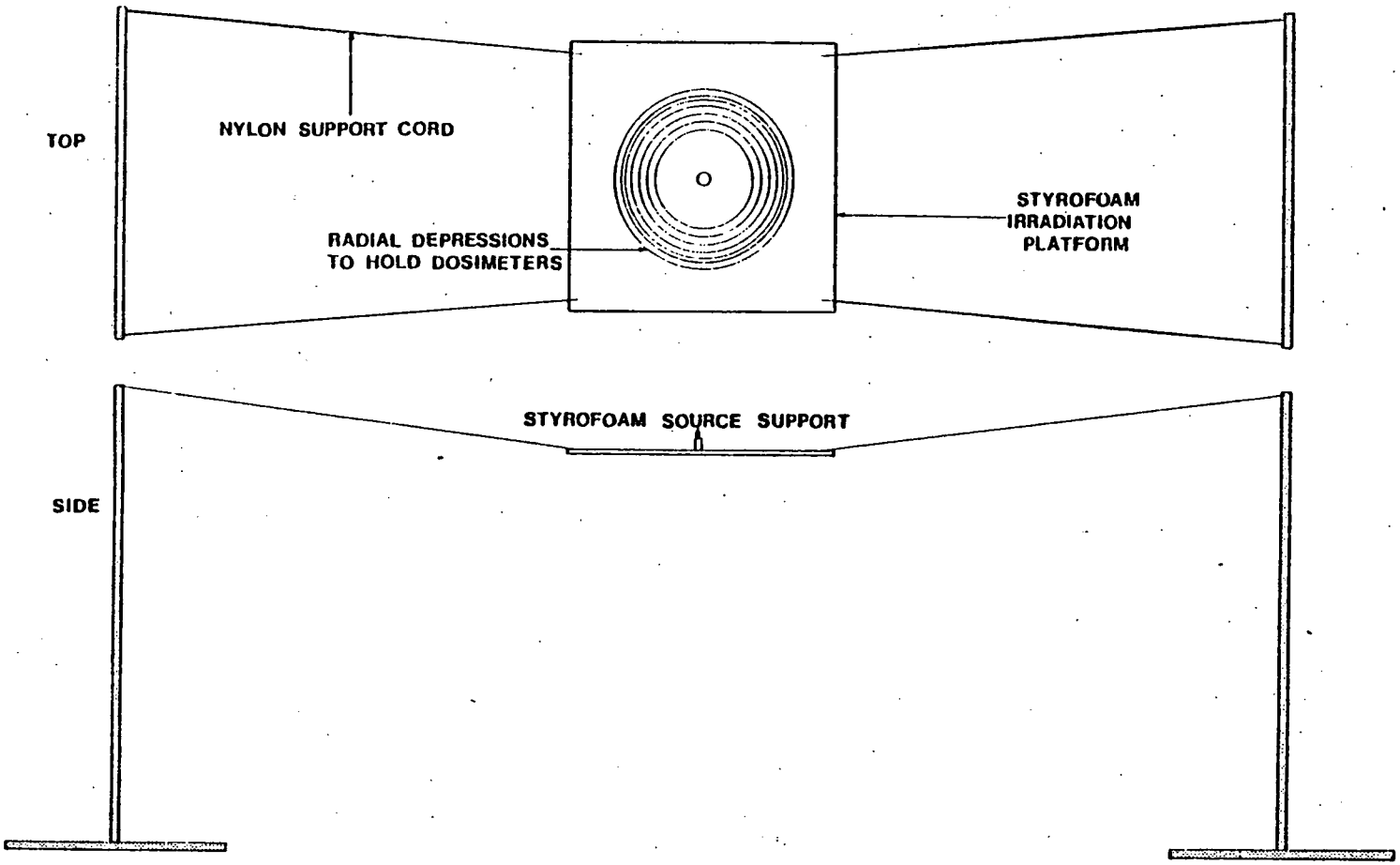

Fig. 5. Diagram showing the irradiation device designed for use with thermoluminescent dosimeters (TLDs).

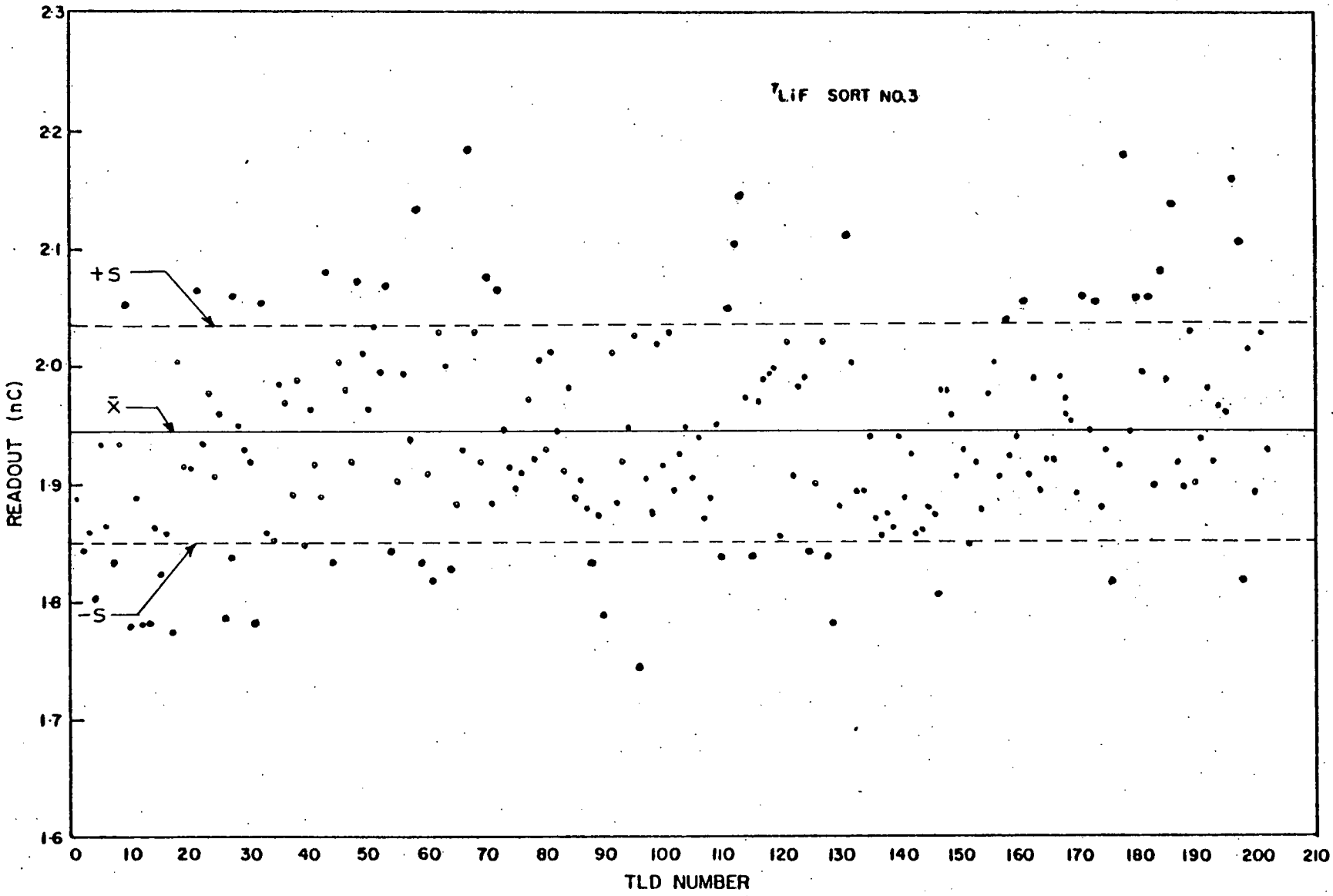

Fig. 6. Sensitivity Data Measured for ^{7}LiF TLDs Exposed to a 3 mCi ^{137}Cs Gamma-Ray Source.

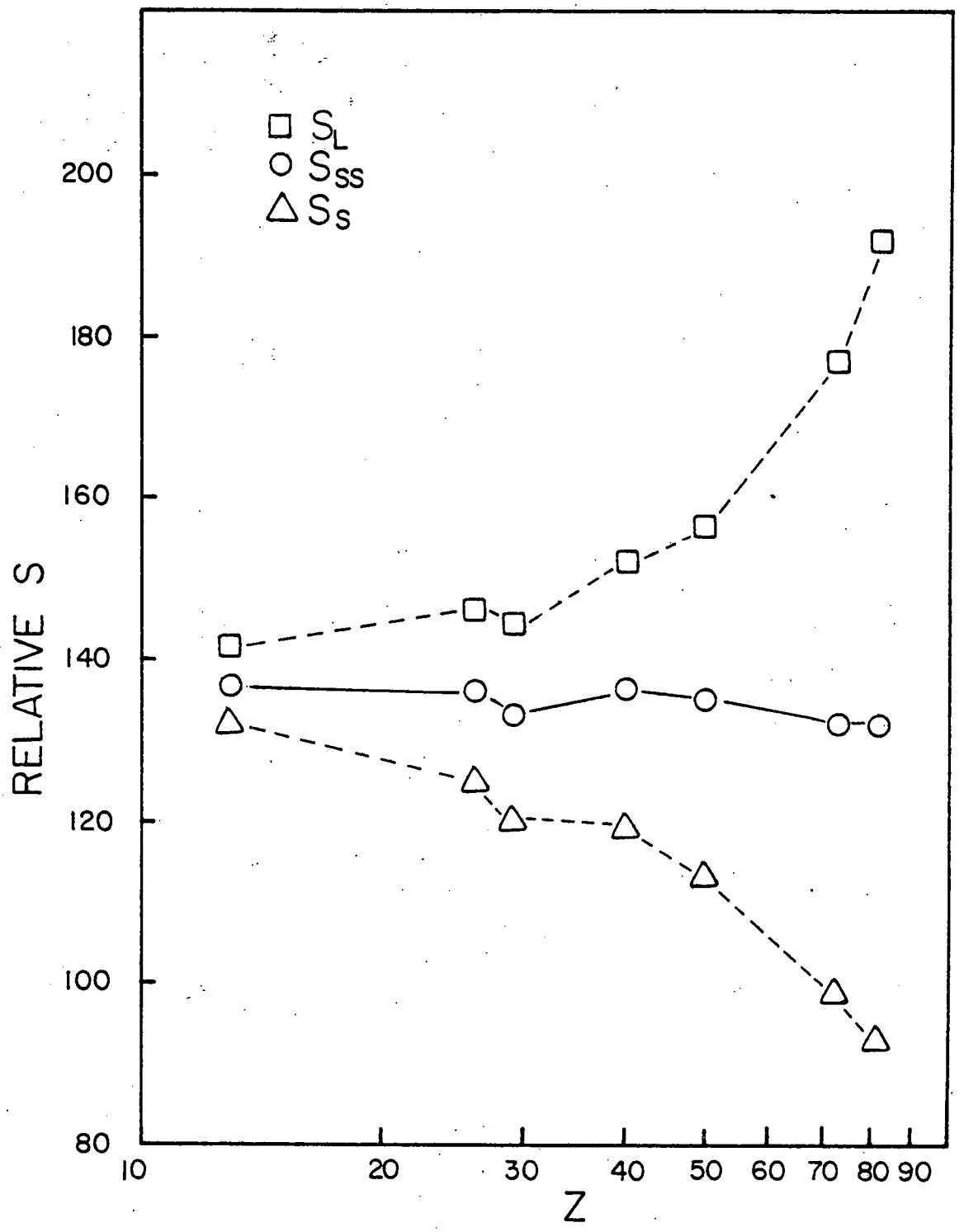

Fig. 7 Relative Number of Source Decays from ^{60}Co Irradiated ^{7}LiF TLDs as a Function of Encasement Material Atomic Number.

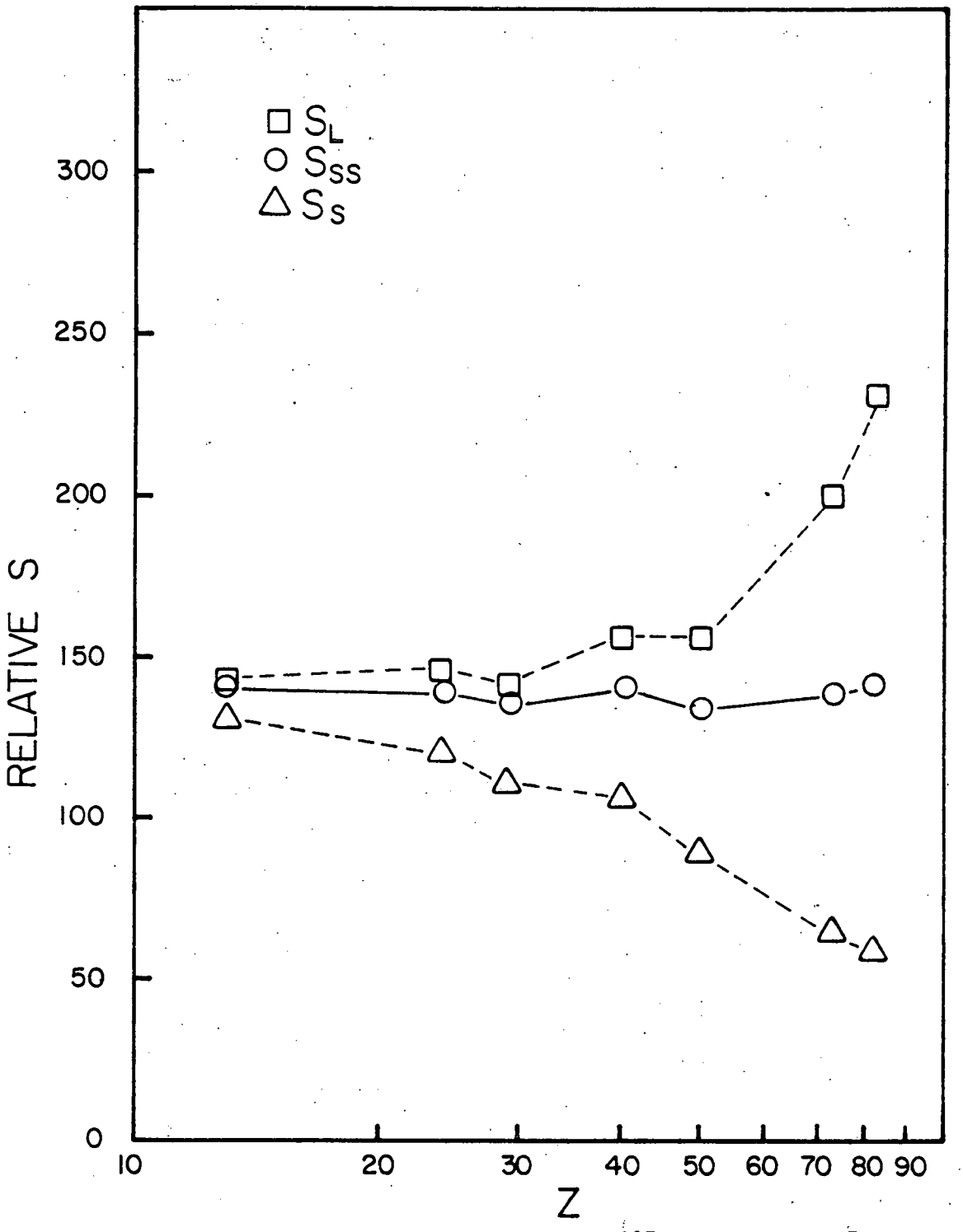

Fig.8 Relative Number of Source Decays from ^{137}Cs Irradiated ^{7}LiF TLDs as a Function of Encasement Material Atomic Number.

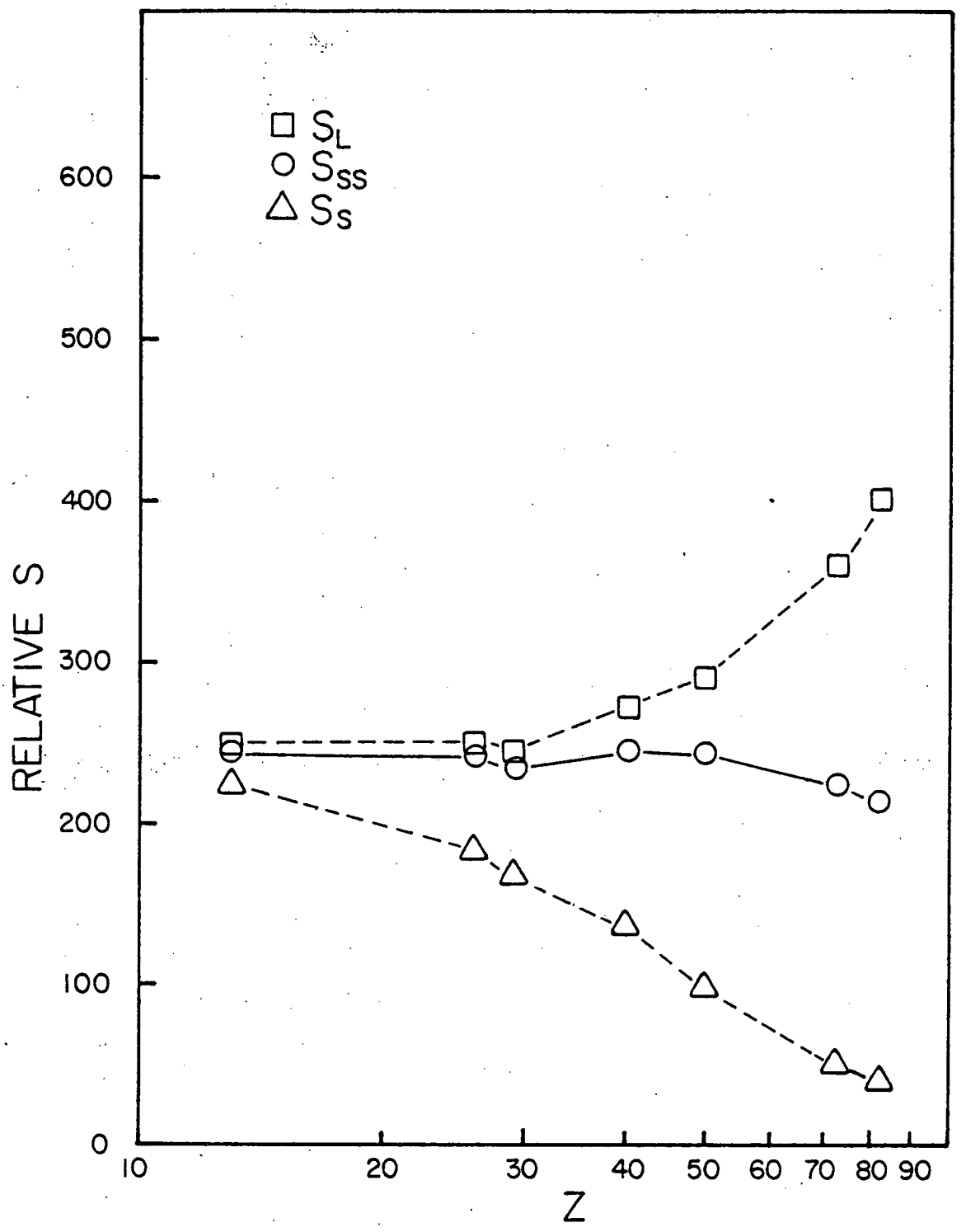

Fig. 9. Relative Number of Source Decays from ^{113}Sn Irradiated ^{7}LiF TLDs as a Function of Encasement Material Atomic Number.

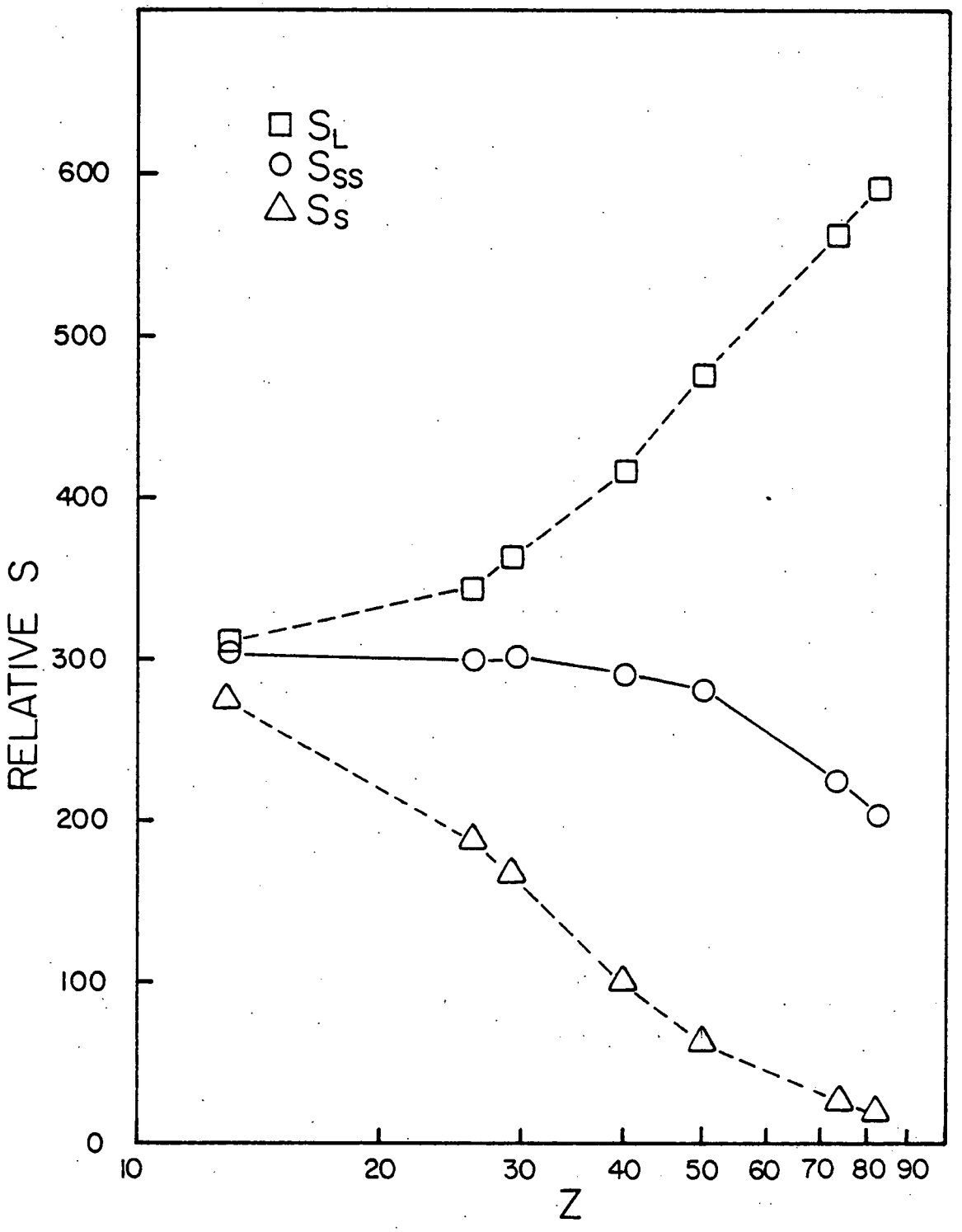

Fig. 10. Relative Number of Source Decays from ^{203}Hg Irradiated ^{7}LiF TLDs as a Function of Encasement Material Atomic Number.

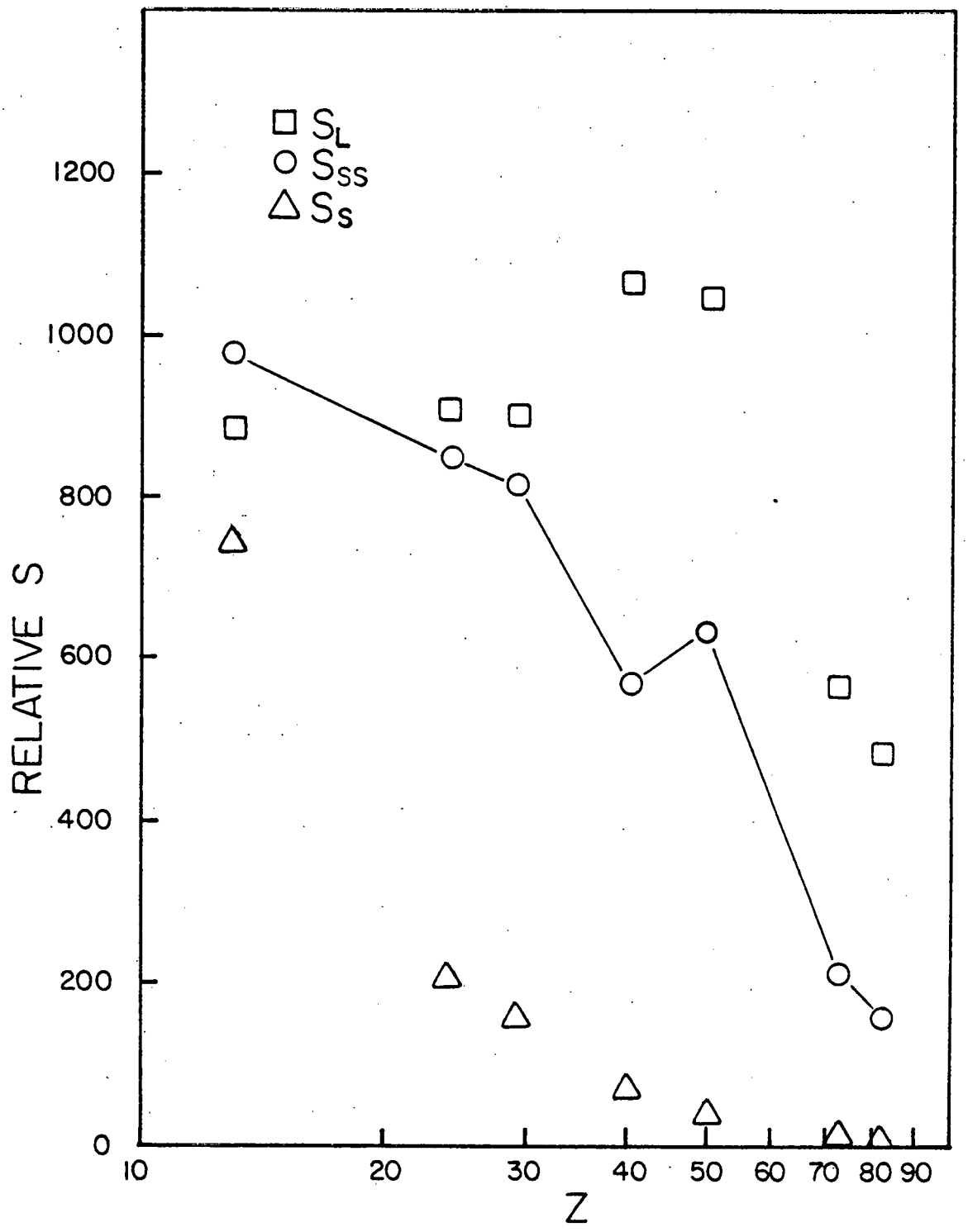

Fig. 11. Relative Number of Source Decays from ^{141}Ce Irradiated ^{7}LiF TLDs as a Function of Encasement Material Atomic Number.

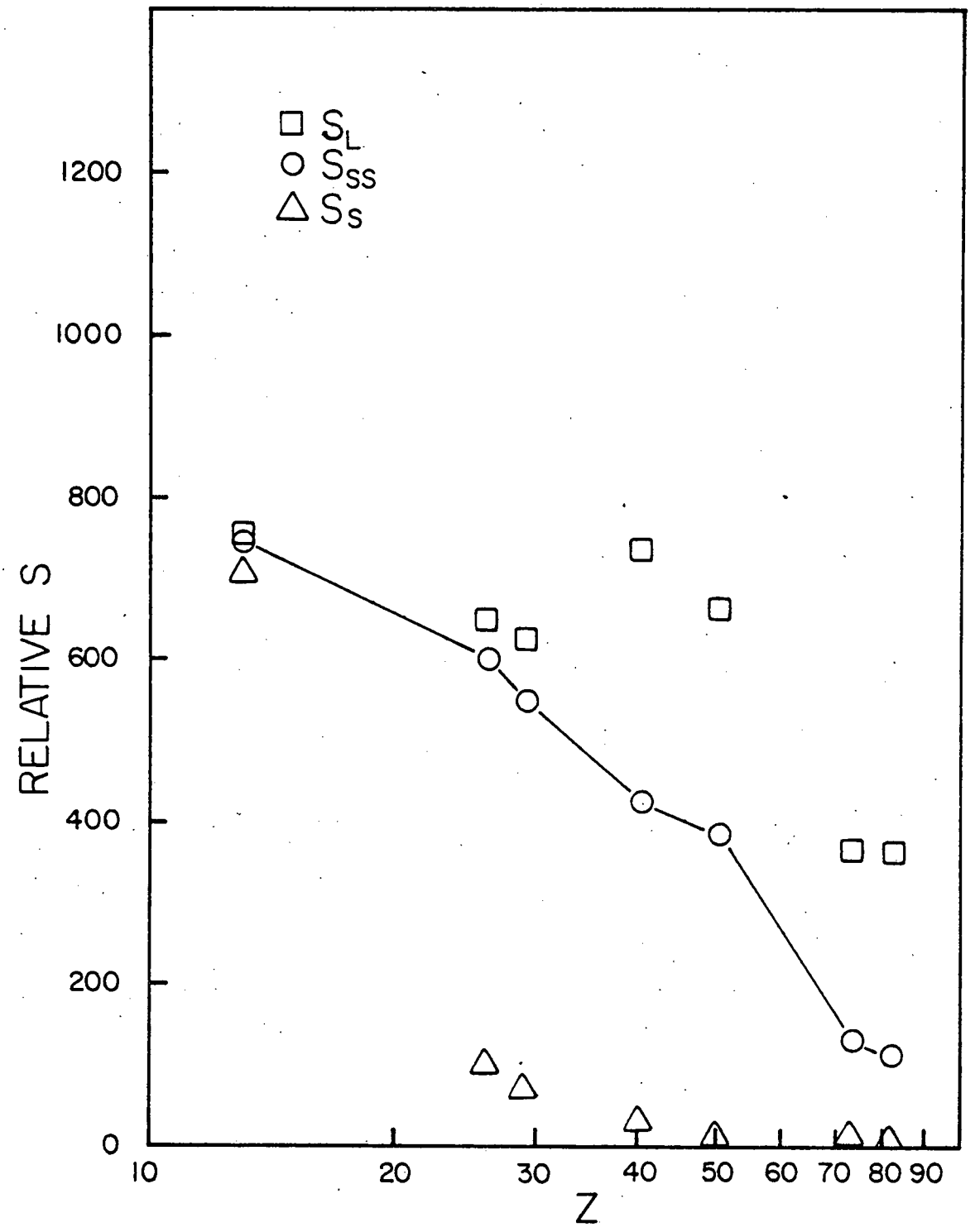

Fig. 12. Relative Number of Source Decays from ^{57}Co Irradiated ^{7}LiF TLDs as a Function of Encasement Material Atomic Number.

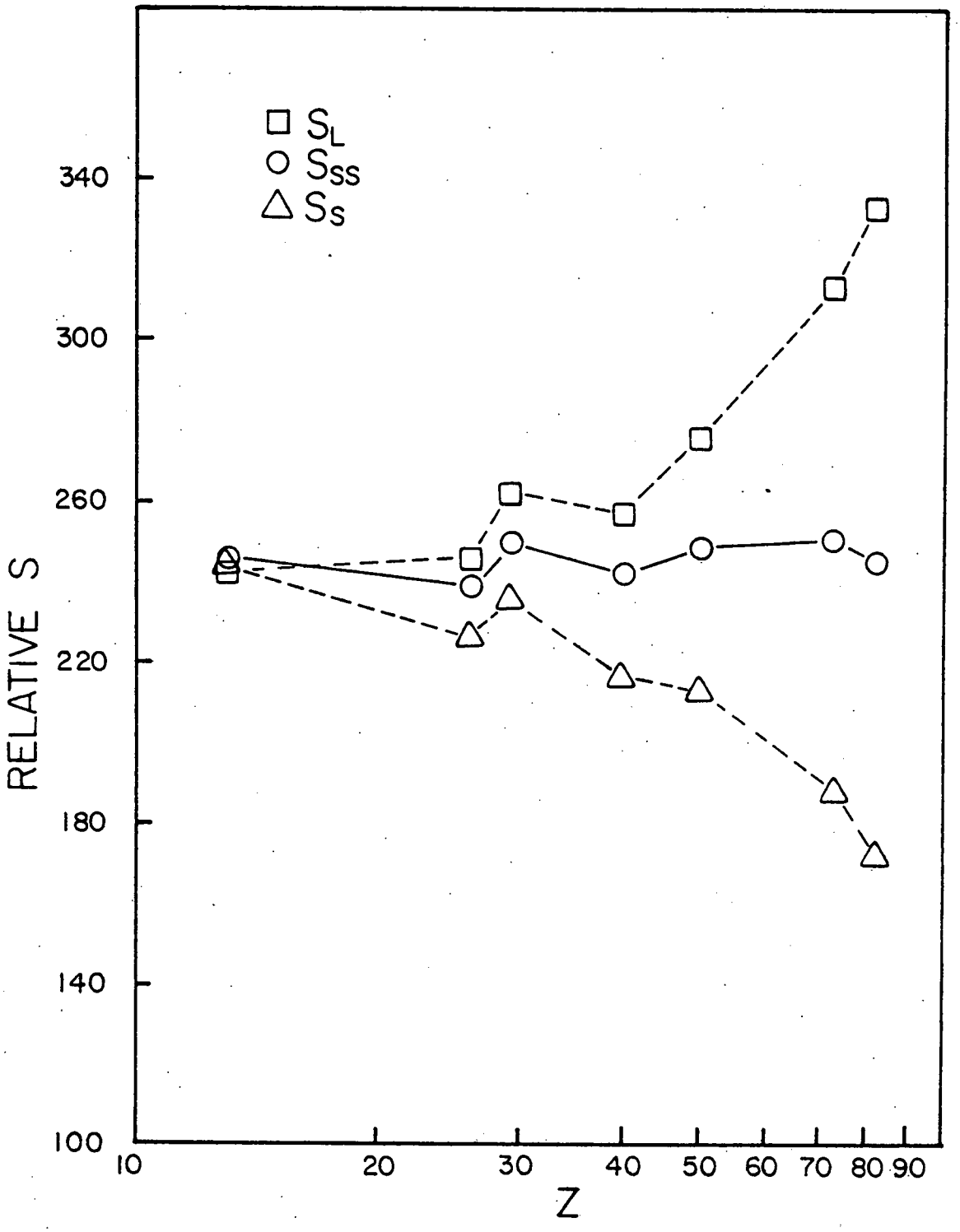

Fig. 13. Relative Number of Source Decays from ^{60}Co Irradiated CaF_2:Mn TLDs as a Function of Encasement Material Atomic Number.

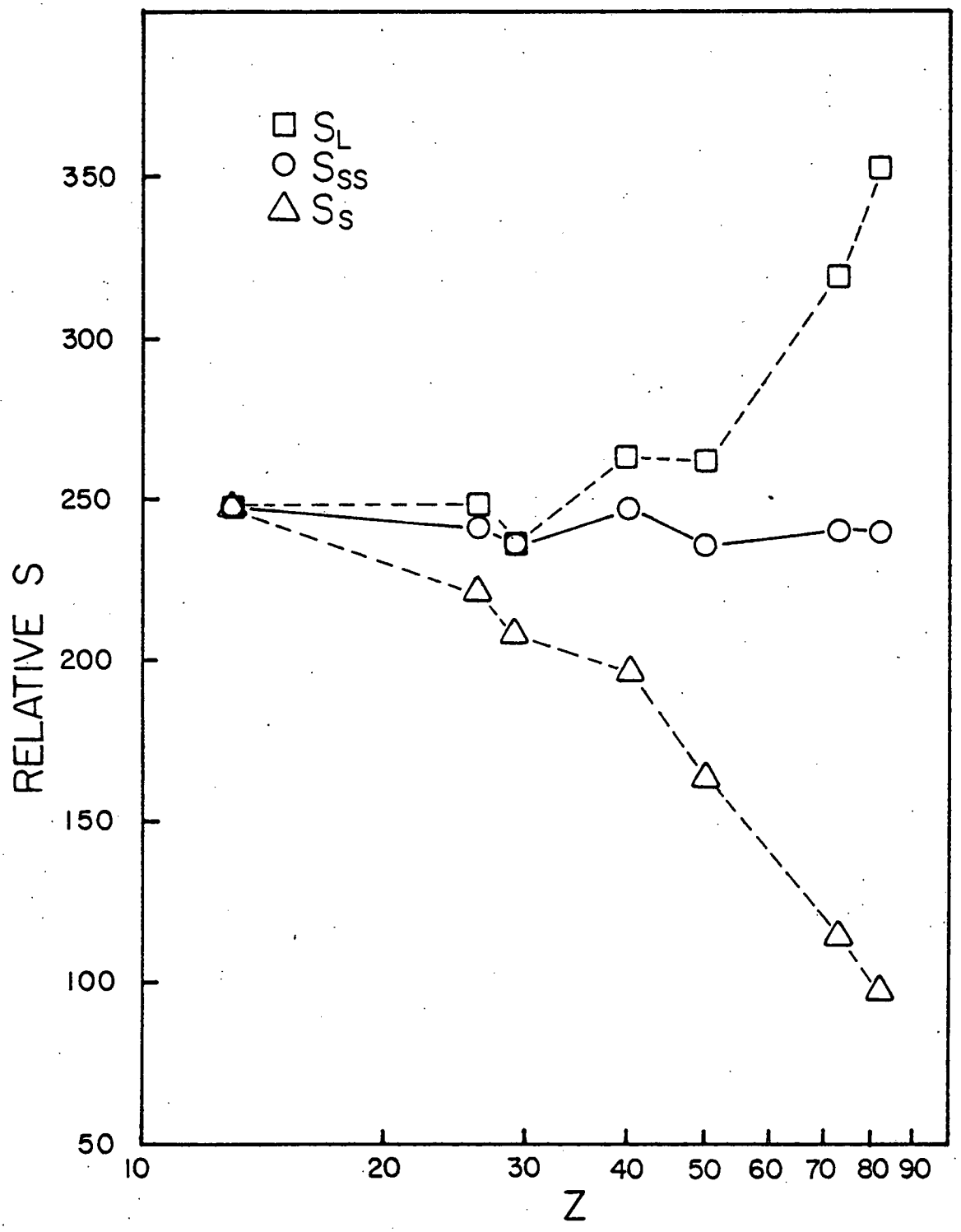

Fig. 14. Relative Number of Source Decays from ^{137}Cs Irradiated CaF_2:Mn TLDs as a Function of Encasement Material Atomic Number.

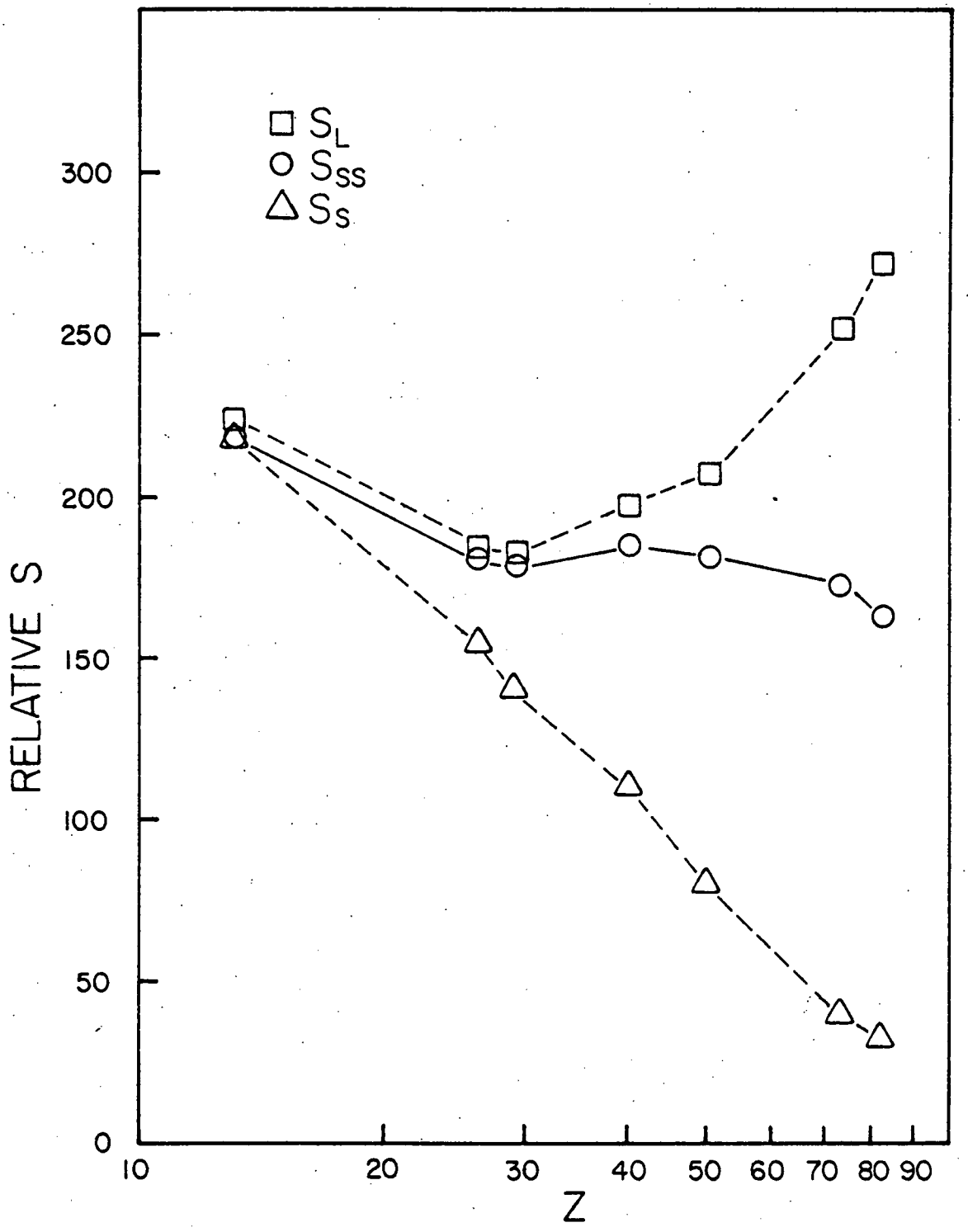

Fig. 15. Relative Number of Source Decays from ^{113}Sn Irradiated CaF_2:Mn TLDs as a Function of Encasement Material Atomic Number.

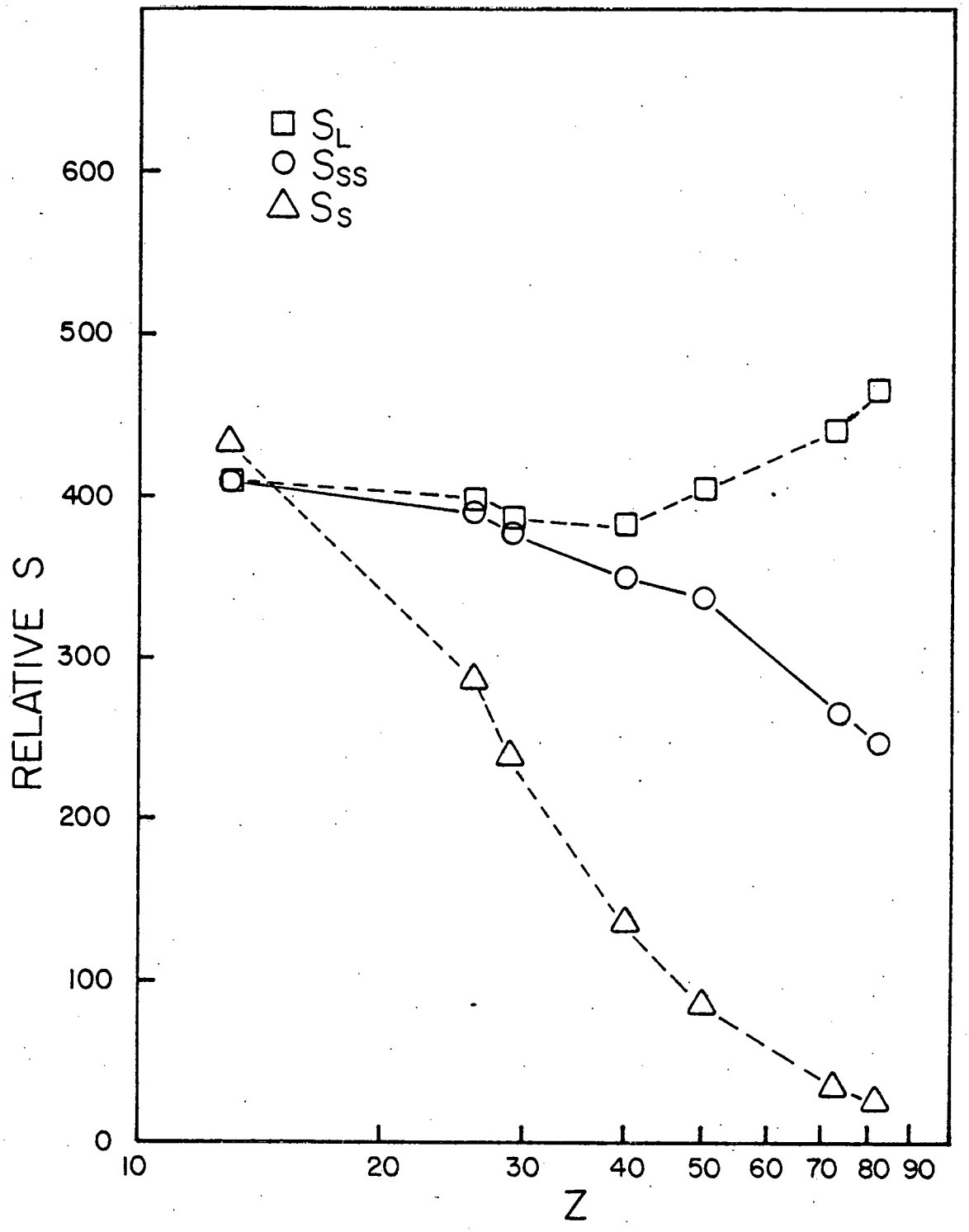

Fig. 16. Relative Number of Source Decays from ^{203}Hg Irradiated CaF_2:Mn TLDs as a Function of Encasement Material Atomic Number.

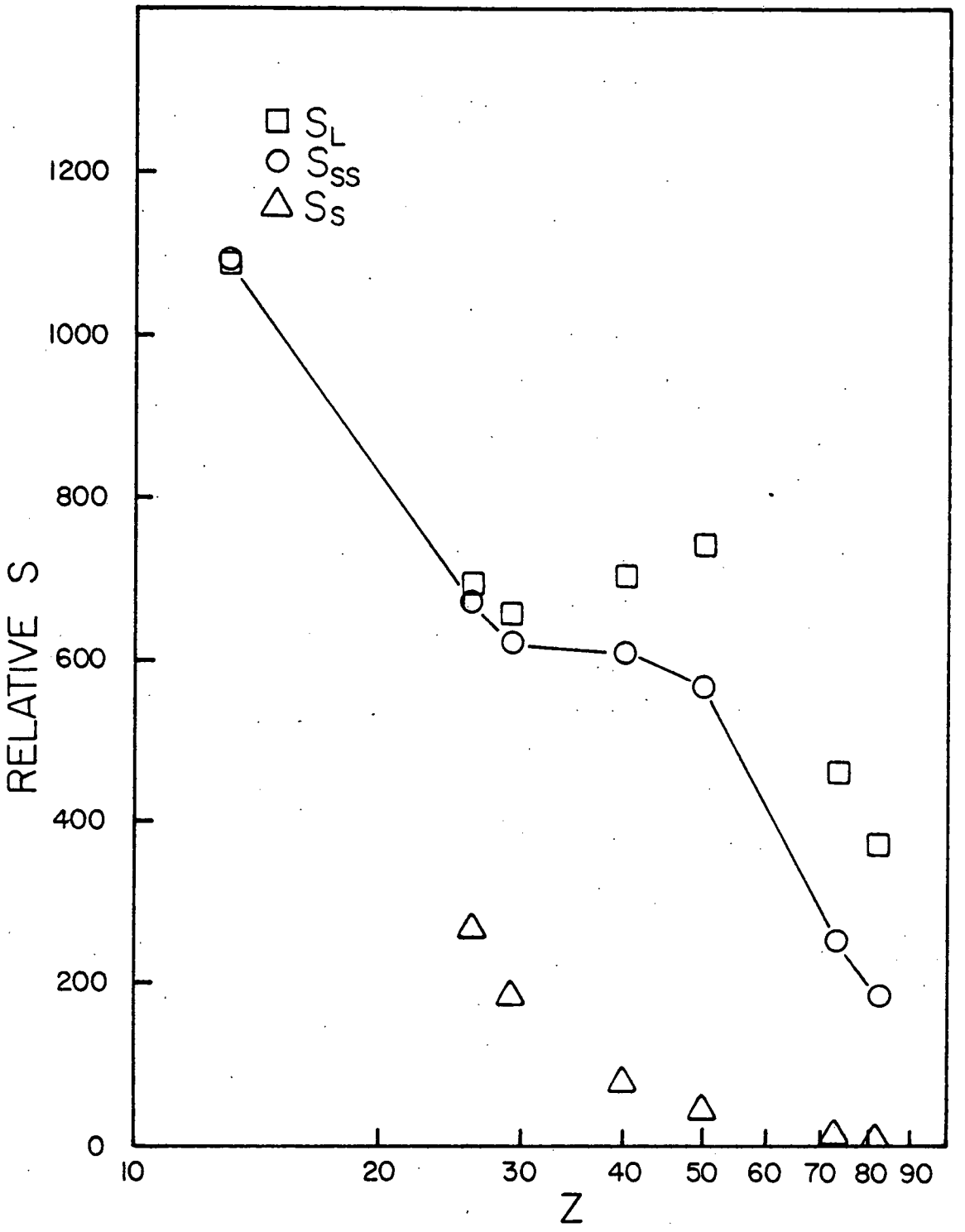

Fig. 17. Relative Number of Source Decays from ^{141}Ce Irradiated CaF_2:Mn TLDs as a Function of Encasement Material Atomic Number.

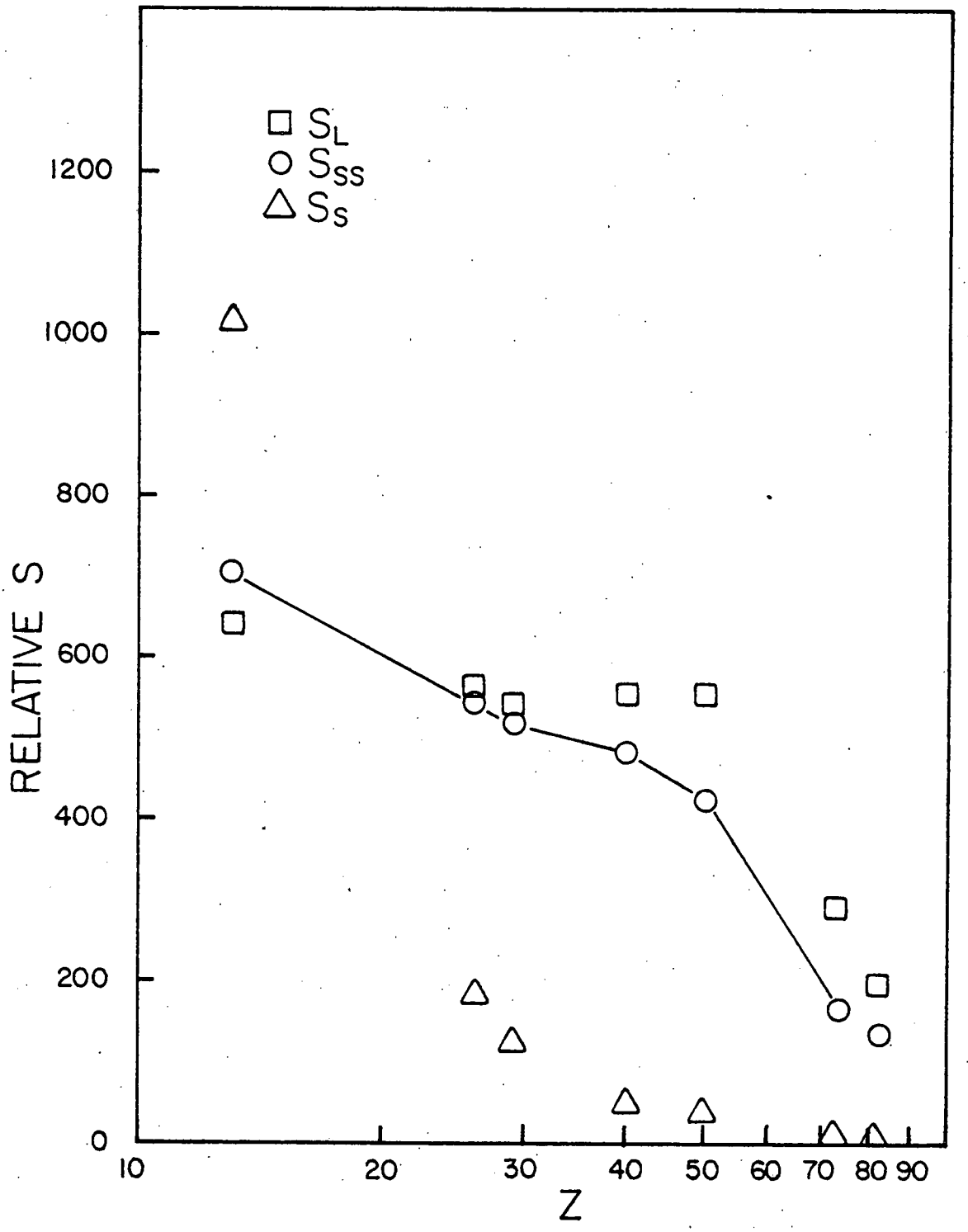

Fig. 18. Relative Number of Source Decays from ^{57}Co Irradiated CaF_2:Mn TLDs as a Function of Encasement Material Atomic Number.

Table I. Partial Compilation of Input Parameter used to Calculate the Dose Ratio [$f(T_\gamma)$] using TERC/III for 1x1x6 mm ^7LiF and CaF_2 TLDs.

Material	<Z/A>[a']	Density ρ (g/cm^3)	Mean Chord[b'] Length, g (g/cm^2)	Ionization[c'] Potential, I (eV)	Density effect Parameters				
					c	a	m	x_0	x_1
^7LiF	0.4616	2.63	0.2430	86.5	-3.07	0.456	2.76	-0.07	2.0
CaF_2	0.4867	3.04	0.2806	158	-4.50	0.100	3.40	0.08	3.0

[a'] Calcuated using the equation: $\langle Z/A \rangle = \sum_j \varepsilon_j \, (Z_j/A_j)$.

For ^7LiF: $\varepsilon_1 = 0.269$, $Z_1 = 3$, $A_1 = 7$, $\varepsilon_2 = 0.731$, $Z_2 = 9$, and $A_2 = 18.9984$

For CaF_2: $\varepsilon_1 = 0.513$, $Z_1 = 20$, $A_1 = 40.08$, $\varepsilon_2 = 0.487$, $Z_2 = 9$, and $A_2 = 18.9984$

[b'] $g = 4V\rho/s$ (g/cm^2)

[c'] $\ln I = (Z/A)^{-1} \sum_j \varepsilon_j \, (Z_j/A_j) \, \ln I_j$

Table II. Partial Compilation of Input Parameters Used to Calculate the Dose Ratio [$f(T_\gamma)$] Using TERC/III for Each Encasement Material

Material	Atomic Number Z	Atomic Weight A	Ionization Potential I (eV)	Density Effect Parameters				
				c	a	m	X_0	X_1
Lead	82	207.2	826.	-6.21	0.355	2.64	0.4	3.0
Tantalum	73	180.9	701	-6.03	0.028	3.91	0.30	4.0
Tin	50	118.7	517	-6.28	0.404	2.52	0.20	3.0
Zirconium	40	91.22	420	-5.39	0.250	2.80	0.20	3.0
Copper	29	63.57	323	-4.43	0.109	3.39	0.20	3.0
Iron	26	55.84	273	-4.62	0.127	3.29	0.10	3.0
Stainless Steel	$25.23^{a'}$	$54.98^{b'}$	$273^{c'}$	-4.62	0.127	3.29	0.10	3.0
Aluminum	13	27	164	-4.21	0.091	3.51	0.05	3.0

$a'_Z = \sum_j E_j Z_j$ where $E_j \equiv$ fraction by weight of the jth element

$b'_A = \sum_j E_j A_j$

$c'_{\ln I} = (Z/A)^{-1} \sum_j E_j \, (Z_j/A_j) \, \ln I_j$

Table III. Comparison of Collision Mass Stopping Power Ratios for LiF Reported by Berger and Seltzer and Calculated using TERC/III.

Electron Energy (MeV)	Collision Mass Stopping Powers (MeV-cm^2/g) Reported by Berger and Seltzer LiF	Calculated in TERC/III LiF	Ratio TERC/III / Berger and Seltzer
0.010	18.17	18.27	1.006
0.015	13.30	13.36	1.005
0.020	10.66	10.71	1.005
0.030	7.823	7.857	1.004
0.040	6.311	6.336	1.004
0.050	5.363	5.384	1.004
0.060	4.711	4.729	1.004
0.080	3.870	3.884	1.004
0.10	3.350	3.362	1.004
0.15	2.639	2.648	1.003
0.20	2.277	2.285	1.004
0.30	1.916	1.922	1.003
0.40	1.742	1.748	1.003
0.50	1.645	1.650	1.003
0.60	1.585	1.590	1.003
0.80	1.521	1.525	1.003
1.0	1.492	1.496	1.003
1.5	1.473	1.477	1.003
2.0	1.478	1.482	1.003
3.0	1.502	1.505	1.002
4.0	1.524	1.528	1.003
5.0	1.544	1.547	1.002
6.0	1.560	1.564	1.003
8.0	1.586	1.590	1.003
10.0	1.606	1.609	1.002

Table IV. Comparison of Collision Mass Stopping Power Ratios for CaF_2 Reported by Attix and Calculated using TERC/III.

Electron Energy (MeV)	Collision Mass Stopping Powers (MeV-cm^2/g)		
	Reported by Attix CaF_2	Calculated in TERC/III CaF_2	Ratio $\left(\frac{\text{TERC/III}}{\text{Attix}}\right)$
0.010	16.65	16.85	1.012
0.015	--	12.46	--
0.020	9.943	10.05	1.011
0.030	--	7.431	--
0.040	--	6.023	--
0.050	5.092	5.136	1.009
0.060	--	4.523	--
0.080	--	3.730	--
0.10	3.213	3.238	1.008
0.15	--	2.56	--
0.20	2.203	2.219	1.007
0.30	--	1.880	--
0.40	--	1.721	--
0.50	1.61	1.634	1.008
0.60	--	1.583	--
0.80	--	1.533	--
1.0	1.488	1.516	1.019
1.5		1.506	--
2.0	1.488	1.517	1.019
3.0	--	1.548	--
4.0	--	1.577	--
5.0	1.571	1.601	1.019
6.0	--	1.621	--
8.0	--	1.653	--
10.0	1.646	1.678	1.019

Table V. Comparison of Collision Mass Stopping Powers for Lead Reported by Berger and Seltzer and Calculated using TERC/III.

Electron Energy (MeV)	Collision Mass Stopping Powers (MeV-cm^2/g) Reported by Berger and Seltzer Lead	Calculated in TERC/III Lead	Ratio TERC/III / Berger and Seltzer
0.010	8.419	8.416	1.000
0.015	6.556	6.554	1.000
0.020	5.450	5.448	1.000
0.030	4.179	4.178	1.000
0.040	3.462	3.461	1.000
0.050	2.997	2.996	1.000
0.060	2.669	2.668	1.000
0.080	2.237	2.237	1.000
0.10	1.964	1.964	1.000
0.15	1.584	1.584	1.000
0.20	1.389	1.388	0.999
0.30	1.196	1.195	0.999
0.40	1.106	1.106	1.000
0.50	1.059	1.059	1.000
0.60	1.033	1.032	0.999
0.80	1.010	1.010	1.000
1.0	1.002	1.001	0.999
1.5	1.015	1.014	0.999
2.0	1.036	1.036	1.000
3.0	1.076	1.076	1.000
4.0	1.109	1.108	0.999
5.0	1.135	1.135	1.000
6.0	1.157	1.157	1.000
8.0	1.191	1.191	1.000
10.0	1.217	1.217	1.000

Table VI. Comparison of Collision Mass Stopping Powers for Tin Reported by Berger and Seltzer and Calculated using TERC/III.

Electron Energy (MeV)	Collision Mass Stopping Powers (MeV-cm^2/g)		
	Reported by Berger and Seltzer Tin	Calculated in TERC/III Tin	Ratio TERC/III / Berger and Seltzer
0.010	10.56	10.55	0.999
0.015	8.061	8.053	0.999
0.020	6.624	6.619	0.999
0.030	5.013	5.009	0.999
0.040	4.120	4.117	0.999
0.050	3.547	3.544	0.999
0.060	3.147	3.145	0.999
0.080	2.623	2.621	0.999
0.10	2.294	2.292	0.999
0.15	1.837	1.836	0.999
0.20	1.604	1.603	0.999
0.30	1.374	1.373	0.999
0.40	1.266	1.266	1.000
0.50	1.208	1.204	0.997
0.60	1.172	1.172	0.997
0.80	1.144	1.143	0.999
1.0	1.134	1.134	1.000
1.5	1.141	1.143	1.002
2.0	1.159	1.164	1.004
3.0	1.197	1.205	1.007
4.0	1.229	1.239	1.008
5.0	1.255	1.267	1.010
6.0	1.277	1.290	1.010
8.0	1.277	1.326	1.012
10.0	1.336	1.354	1.013

Table VII. Comparison of Collision Mass Stopping Powers for Copper Reported by Berger and Seltzer and Calculated using TERC/III.

Electron Energy (MeV)	Collision Mass Stopping Powers (MeV-cm^2/g)		
	Reported by Berger and Seltzer Copper	Calculated in TERC/III Copper	Ratio TERC/III / Berger and Seltzer
0.010	13.28	13.16	0.991
0.015	9.973	9.894	0.992
0.020	8.120	8.059	0.992
0.030	6.078	6.036	0.993
0.040	4.962	4.929	0.993
0.050	4.252	4.225	0.994
0.060	3.759	3.736	0.994
0.080	3.118	3.099	0.994
0.10	2.711	2.701	0.994
0.15	2.164	2.152	0.994
0.20	1.882	1.872	0.995
0.30	1.603	1.596	0.996
0.40	1.473	1.467	0.996
0.50	1.396	1.390	0.996
0.60	1.353	1.348	0.996
0.80	1.310	1.305	0.996
1.0	1.293	1.289	0.997
1.5	1.291	1.287	0.997
2.0	1.305	1.302	0.998
3.0	1.338	1.355	0.998
4.0	1.367	1.365	0.999
5.0	1.391	1.389	0.999
6.0	1.411	1.409	0.999
8.0	1.442	1.440	0.999
10.0	1.466	1.464	0.999

Table VIII. Comparison of Collision Mass Stopping Powers for Iron Reported by Berger and Seltzer and Calculated using TERC/III.

Electron Energy (MeV)	Collision Mass Stopping Powers (MeV-cm^2/g)		
	Reported by Berger and Seltzer Iron	Calculated in TERC/III Iron	Ratio TERC/III / Berger and Seltzer
0.010	14.07	14.07	1.000
0.015	10.53	10.53	1.000
0.020	8.553	8.551	1.000
0.030	6.385	6.384	1.000
0.040	5.204	5.203	1.000
0.050	4.455	4.454	1.000
0.060	3.935	3.934	1.000
0.080	3.259	3.258	1.000
0.10	2.828	2.837	1.000
0.15	2.257	2.257	1.000
0.20	1.961	1.961	1.000
0.30	1.667	1.669	1.001
0.40	1.526	1.526	1.000
0.50	1.449	1.452	1.002
0.60	1.403	1.407	1.003
0.80	1.356	1.362	1.004
1.0	1.337	1.345	1.006
1.5	1.333	1.343	1.008
2.0	1.346	1.358	1.009
3.0	1.378	1.393	1.011
4.0	1.406	1.423	1.012
5.0	1.430	1.448	1.013
6.0	1.450	1.469	1.013
8.0	1.481	1.502	1.014
10.0	1.505	1.527	1.015

Table IX. Comparison of Collision Mass Stopping Powers for Aluminum Reported by Berger and Seltzer and Calculated using TERC/III.

Electron Energy (MeV)	Collision Mass Stopping Powers (MeV-cm^2/g) Reported by Berger and Seltzer Aluminum	Calculated in TERC/III Aluminum	Ratio TERC/III / Berger and Seltzer
0.010	16.57	16.56	0.999
0.015	12.25	12.23	0.998
0.020	9.885	9.862	0.998
0.030	7.316	7.300	0.998
0.040	5.932	5.919	0.998
0.050	5.059	5.048	0.998
0.060	4.456	4.447	0.998
0.080	3.676	3.668	0.998
0.10	3.191	3.185	0.998
0.15	2.526	2.521	0.998
0.20	2.188	2.183	0.998
0.30	1.848	1.844	0.998
0.40	1.691	1.687	0.998
0.50	1.603	1.600	0.998
0.60	1.551	1.548	0.998
0.80	1.496	1.493	0.998
1.0	1.473	1.470	0.998
1.5	1.464	1.462	0.999
2.0	1.476	1.473	0.998
3.0	1.508	1.505	0.998
4.0	1.537	1.534	0.998
5.0	1.561	1.558	0.998
6.0	1.581	1.578	0.998
8.0	1.613	1.610	0.998
10.0	1.637	1.635	0.999

Table X. Collision Mass Stopping Powers for Tantalum, Zirconium, and Stainless Steel Calculated Using TERC/III.

Electron Energy (MeV)	Collision Mass Stopping Powers (MeV-cm^2/g)		
	Tantalum	Zirconium	Stainless Steel
0.010	9.117	11.72	13.86
0.015	7.045	8.884	10.37
0.020	5.831	7.270	8.428
0.030	4.449	5.475	6.291
0.040	3.674	4.486	5.128
0.050	3.174	3.855	4.390
0.060	2.823	3.415	3.211
0.080	2.361	2.839	3.211
0.10	2.070	2.479	2.796
0.15	1.665	1.981	2.224
0.20	1.458	1.727	1.932
0.30	1.253	1.476	1.645
0.40	1.157	1.358	1.504
0.50	1.107	1.295	1.431
0.60	1.078	1.258	1.387
0.80	1.050	1.221	1.343
1.0	1.045	1.209	1.326
1.5	1.057	1.212	1.324
2.0	1.078	1.230	1.338
3.0	1.117	1.267	1.373
4.0	1.149	1.299	1.403
5.0	1.175	1.325	1.427
6.0	1.196	1.347	1.448
8.0	1.229	1.381	1.480
10.0	1.254	1.407	1.505

Table XI. Comparison of Mass Energy Absorption Coefficients for Lithium Fluoride Reported by Sinclair and those used in TERC/III.

Gamma-ray Energy (MEV)	μ_{en}/ρ (cm^2/g) Reported by Sinclair[a] LiF	Used in TERC/III[b] ^{7}LiF	TERC/III / Sinclair
0.01	5.61	5.73	1.021
0.015	1.51	1.56	1.033
0.02	0.607	0.629	1.036
0.03	0.174	0.1777	1.017
0.04	0.0763	0.0767	1.005
0.05	0.0448	0.0439	0.980
0.06	0.0323	0.0317	0.981
0.08	0.0240	0.0234	0.975
0.10	0.0224	0.219	0.978
0.15	0.0234	0.0231	0.987
0.20	0.0249	0.0248	0.996
0.30	0.0266	0.0266	1.000
0.40	0.0274	0.0273	0.996
0.50	0.0276	0.0276	1.000
0.60	0.0274	0.0273	0.996
0.80	0.0267	0.0266	0.996
1.0	0.0258	0.0257	0.996
1.5	0.0236	0.0235	0.996
2	0.0217	0.0217	1.000
3	0.0190	0.0191	1.005
4	0.0174	0.0174	1.006
5	0.0161	0.0161	1.000
6	0.0152	0.0154	1.013
8	0.0141	0.0142	1.007
10	0.0134	0.0137	1.022

[a] W. K. Sinclair, "Radiobiology Dosimetry," Radiation Dosimetry, Vol. III, p. 625.

[b] From E. Storm and H. I. Israel, Nuclear Data Tables, A7, 565 (1970). Wt %: ^{7}Li = 0.269 F = 0.731.

Table XII. Comparison of Mass Energy Absorption Coefficients for CaF_2 Reported by Attix and those used in TERC/III.

Gamma-ray Energy (MeV)	μ_{en}/ρ (cm^2/g) Reported by Attix[a]	μ_{en}/ρ (cm^2/g) Used in TERC/III[b]	TERC/III Attix
0.01	50.70	48.21	0.951
0.015	15.70	15.22	0.969
0.20	6.66	6.60	0.991
0.03	1.96	1.95	0.995
0.04	0.818	0.822	1.005
0.05	0.419	0.425	1.014
0.06	0.247	0.247	1.000
0.08	0.114	0.111	0.974
0.10	0.0677	0.0658	0.972
0.15	0.0373	0.0362	0.971
0.20	0.0315	0.0309	0.981
0.30	0.0296	0.0294	0.993
0.40	0.0295	0.0293	0.993
0.50	0.0293	0.0294	1.003
0.60	0.0290	0.0289	0.997
0.80	0.0281	0.0280	0.996
1.00	0.0271	0.0271	1.000
1.25	0.0259	0.0259	1.000
1.50	0.0248	0.0248	1.000
2.00	0.0229	0.0230	1.004
3.00	0.0205	0.0206	1.005
4.00	0.0192	0.0193	1.005
5.00	0.0184	0.0185	1.005
6.00	0.0179	0.0181	1.011
8.00	0.0175	0.0181	1.034
10.00	0.0173	0.0178	1.029

[a] F. H. Attix, "Thermoluminescence Dosimetry with Calcium Fluoride," Manual on Radiation Dosimetry,, Eds. N. W. Holm and R. J. Berry, Marcel Dekker, Inc., New York (1969).

[b] From E. Storm and H. I. Israel, Nuclear Data Tables A7, 565 (1970). Wt %: Ca = 0.513 F = 0.487.

Table XIII. Mass Energy Absorption Coefficients and Resulting Dose Ratios Calculated using TERC/III for 1x1x6 mm ^{7}LiF TLDs Encased in Various Materials

Nuclide	Gamma-ray Energy, T_γ (MeV)	Mass Energy Absorption Coefficient $[\mu_{en}(T_\gamma)/\rho]_M$ (cm^2/g)	Calculated Dose Ratio $f(T_\gamma)$
	Encasement material (M) of Lead, Z = 82		
Co-57	0.122	1.7480	0.04597
Ce-141	0.145	1.2483	0.06002
Hg-203	0.279	0.3359	0.1902
Sn-113	0.393	0.1518	0.3425
Cs-137	0.662	0.06444	0.6929
Co-60	1.173	0.03423	1.0931
	1.333	0.03099	1.1589
	Encasement Material (M) of Tantalum, Z = 73		
Co-57	0.122	1.6679	0.04552
Ce-141	0.145	1.0892	0.06069
Hg-203	0.279	0.2634	0.2071
Sn-113	0.393	0.1176	0.3810
Cs-137	0.662	0.05263	0.7508
Co-60	1.173	0.03040	1.1179
	1.333	0.02803	1.1712
	Encasement Material (M) of Tin, Z = 50		
Co-57	0.122	0.8543	0.06031
Ce-141	0.145	0.4955	0.08485
Hg-203	0.279	0.1079	0.3450
Sn-113	0.393	0.05413	0.6111
Cs-137	0.662	0.03295	0.9619
Co-60	1.173	0.02485	1.1705
	1.333	0.02376	1.1938
	Encasement Material (M) of Zirconium, Z = 40		
Co-57	0.122	0.4985	0.08318
Ce-141	0.145	0.2846	0.1200
Hg-203	0.279	0.06761	0.4790
Sn-113	0.393	0.04010	0.7565
Cs-137	0.662	0.02950	1.0135
Co-60	1.173	0.02456	1.1365
	1.333	0.02372	1.1501
	Encasement Material (M) of Copper, Z = 29		
Co-57	0.122	0.2092	0.1604
Ce-141	0.145	0.1214	0.2346
Hg-203	0.279	0.04061	0.07071
Sn-113	0.393	0.03159	0.9063
Cs-137	0.662	0.02793	1.0281
Co-60	1.173	0.02481	1.0885
	1.333	0.02407	1.0964

Table XIII. (continued)

	Encasement Material (M) of Iron, Z = 26		
Co-57	0.122	0.1557	0.2031
Ce-141	0.145	0.09245	0.2953
Hg-203	0.279	0.03655	0.7653
Sn-113	0.393	0.03055	0.9254
Cs-137	0.662	0.02808	1.0115
Co-60	1.173	0.02523	1.0570
	1.333	0.02452	1.0626
	Encasement Material (M) of Stainless Steel		
Co-57	0.122	0.1526	0.2068
Ce-141	0.145	0.09075	0.3005
Hg-203	0.279	0.03628	0.7710
Sn-113	0.393	0.03055	0.9270
Cs-137	0.662	0.02805	1.0158
Co-60	1.173	0.02529	1.0614
	1.333	0.02457	1.0679
	Encasement Material (M) of Aluminum, Z = 13		
Co-57	0.122	0.03305	0.7011
Ce-141	0.145	0.02873	0.8125
Hg-203	0.279	0.02785	0.9506
Sn-111	0.393	0.02855	0.9655
Cs-137	0.662	0.02821	0.9791
Co-60	1.173	0.02597	0.9924
	1.333	0.02520	0.9958

Table XIV. Mass Energy Absorption Coefficients and Resulting Dose Ratios Calculated using TERC/III for 1x1x6 mm CaF_2 TLDs Encased in Various Materials

Nuclide	Gamma-ray Energy, T_γ (MeV)	Mass Energy Absorption Coefficient $[\mu_{en}(T_\gamma)/\rho]_M$ (cm^2/g)	Calculated Dose Ratio $f(T_\gamma)$
	Encasement material (M) of Lead, Z = 82		
Co-57	0.122	1.7480	0.05622
Ce-141	0.145	1.2483	0.06489
Hg-203	0.279	0.3359	0.1824
Sn-113	0.393	0.1518	0.3278
Cs-137	0.662	0.06444	0.6694
Co-60	1.173	0.03423	1.080
	1.333	0.03099	1.145
	Encasement Material (M) of Tantalum, Z = 73		
Co-57	0.122	1.6679	0.05709
Ce-141	0.145	1.0892	0.06792
Hg-203	0.279	0.2634	0.2033
Sn-113	0.393	0.1176	0.3721
Cs-137	0.662	0.05263	0.7372
Co-60	1.173	0.03040	1.108
	1.333	0.02803	1.163
	Encasement Material (M) of Tin, Z = 50		
Co-57	0.122	0.8543	0.08955
Ce-141	0.145	0.4955	0.1102
Hg-203	0.279	0.1079	0.3624
Sn-113	0.393	0.05413	0.6267
Cs-137	0.662	0.03295	0.9739
Co-60	1.173	0.02485	1.179
	1.333	0.02376	1.202
	Encasement Material (M) of Zirconium, Z = 40		
Co-57	0.122	0.4985	0.1373
Ce-141	0.145	0.2846	0.1693
Hg-203	0.279	0.06761	0.5163
Sn-113	0.393	0.04010	0.7881
Cs-137	0.662	0.02950	1.035
Co-60	1.173	0.02456	1.149
	1.333	0.02372	1.162
	Encasement Material (M) of Copper, Z = 29		
Co-57	0.122	0.2092	0.2949
Ce-141	0.145	0.1214	0.3577
Hg-203	0.279	0.04061	0.7777
Sn-113	0.393	0.03153	0.9545
Cs-137	0.662	0.02793	1.057
Co-60	1.173	0.02481	1.106
	1.333	0.02407	1.112

Table XIV. (continued)

	Encasement Material (M) of Iron, Z = 26		
Co-57	0.122	0.1557	0.3840
Ce-141	0.145	0.09245	0.4581
Hg-203	0.279	0.03655	0.8457
Sn-113	0.393	0.03055	0.9771
Cs-137	0.662	0.02808	1.042
Co-60	1.173	0.02523	1.075
	1.333	0.02452	1.079
	Encasement Material (M) of Stainless Steel		
Co-57	0.122	0.1526	0.3914
Ce-141	0.145	0.09075	0.4663
Hg-203	0.279	0.03628	0.8520
Sn-113	0.393	0.03055	0.9784
Cs-137	0.662	0.02805	1.046
Co-60	1.173	0.02529	1.080
	1.333	0.02457	1.084
	Encasement Material (M) of Aluminum, Z = 13		
Co-57	0.122	0.03305	1.557
Ce-141	0.145	0.02873	1.343
Hg-203	0.279	0.02785	1.061
Sn-111	0.393	0.02856	1.025
Cs-137	0.662	0.02821	1.014
Co-60	1.173	0.02597	1.015
	1.333	0.02520	1.017

Table XV. Five-Millicurie Gamma-ray Sources Purchased for use in the TLD Energy Response Study.

Nuclide	Half-Life	Gamma-ray Energy, MeV	Calibration
Co-57	270 D	0.122, 0.136	± 10%
Ce-141	32.5 D	0.145	± 10%
Hg-203	47 D	0.279	± 10%
Sn-113	115 D	0.393	± 10%
Cs-137	30 Y	0.662	± 4%
Co-60	5.3 Y	1.173, 1.333	± 4.5%

Table XVI Encasement Materials Used During Measurement of the Energy Response of Encased ^{7}LiF and CaF_2 TLDs.

Material	Quantity	Atomic Number	Density (g/cm^3)	Hole Diameter (cm)	Wall Thickness (g/cm^2)
Lead	10	82	11.34	0.022	0.734
Tantalum	10	73	16.60	0.022	0.696
Tin	10	50	7.30	0.022	0.608
Zirconium	10	40	6.50	0.023	0.541
Copper	10	29	8.96	0.025	0.694
Iron	10	26	7.87	0.022	0.656
Stainless Steel	10	Std ANL Sleeves	7.80	0.022	0.693
Aluminum	10	13	2.70	0.022	0.514

Table XVII. TLD Analyzer Output Normalized to Iron Encased ^{7}LiF TLD's from a Precision Subset

Sleeve Material	Z	Normalized TLD Readout (nc) ± $\sigma_{\bar{x}}$ Gamma-ray Energy (MeV)					
		0.136 (11%) 0.122 (87%)	0.145	0.279	0.393	0.662	1.173 (100%) 1.333 (100%)
Lead	82	0.486±0.010	0.508±0.008	1.559±0.018	1.657±0.025	1.613±0.029	1.354±0.020
Tantalum	73	0.520±0.016	0.612±0.021	1.485±0.024	1.487±0.025	1.396±0.023	1.245±0.023
Tin	50	1.041±0.013	1.156±0.020	1.259±0.016	1.185±0.012	1.077±0.015	1.086±0.020
Zirconium	40	1.168±0.014	1.182±0.014	1.128±0.017	1.091±0.017	1.058±0.013	1.051±0.012
Copper	29	0.955±0.020	1.001±0.014	1.037±0.015	0.985±0.012	0.976±0.010	0.997±0.012
Iron	26	1.000±0.010	1.000±0.015	1.000±0.014	1.000±0.009	1.000±0.013	1.000±0.013
Stainless	--	0.992±0.014	0.971±0.016	1.007±0.012	1.002±0.012	1.005±0.015	0.994±0.014
Aluminum	13	0.922±0.012	0.987±0.014	0.970±0.019	0.997±0.012	0.981±0.013	0.974±0.015

Table XVIII. TLD Analyzer Output Normalized to Iron Encased CaF_2:Mn TLD's from a Precision Subset

Sleeve Material	Z	Normalized TLD Readout (nc) ± $\sigma_{\bar{x}}$					
		Gamma-ray Energy (MeV)					
		0.136 (11%) 0.122 (87%)	0.145	0.279	0.393	0.662	1.173 (100%) 1.333 (100%)
Lead	82	0.401±0.008	0.523±0.008	1.262±0.018	1.526±0.024	1.464±0.021	1.380±0.019
Tantalum	73	0.492±0.019	0.660±0.012	1.204±0.021	1.412±0.016	1.319±0.015	1.306±0.025
Tin	50	0.999±0.015	1.088±0.013	1.103±0.014	1.149±0.021	1.074±0.016	1.133±0.012
Zirconium	40	1.002±0.019	0.989±0.022	1.016±0.016	1.082±0.019	1.062±0.014	1.048±0.017
Copper	29	0.977±0.016	0.952±0.007	0.987±0.015	1.002±0.015	0.986±0.010	1.072±0.017
Iron	26	1.000±0.018	1.000±0.010	1.000±0.015	1.000±0.017	1.000±0.013	1.000±0.016
Stainless	--	1.002±0.015	0.995±0.012	0.982±0.014	1.006±0.015	1.009±0.012	1.002±0.014
Aluminum	13	1.022±0.015	1.482±0.017	0.987±0.012	1.184±0.019	1.001±0.011	1.003±0.016

Table XIX. TLD Analyzer Output Normalized to Iron Encased 1x1x6 mm ^{7}LiF TLD's Corrected for Individual Sensitivity

Sleeve Material	Z	Normalized Sensitivity Corrected TLD Readout (nc) ± $\sigma_{\bar{x}}$					
		Gamma-ray Energy (MeV)					
		0.136 (11%) 0.122 (87%)	0.145	0.279	0.393	0.662	1.173 (100%) 1.333 (100%)
Lead	82	0.484±0.009	0.504±0.008	1.543±0.027	1.634±0.020	1.604±0.020	1.337±0.018
Tantalum	73	0.521±0.008	0.606±0.016	1.472±0.026	1.474±0.022	1.391±0.016	1.231±0.015
Tin	50	1.042±0.016	1.155±0.014	1.251±0.022	1.178±0.012	1.076±0.014	1.078±0.016
Zirconium	40	1.171±0.014	1.186±0.013	1.122±0.023	1.093±0.013	1.063±0.012	1.047±0.015
Copper	29	0.978±0.013	0.999±0.012	1.032±0.018	0.993±0.010	0.976±0.013	0.991±0.013
Iron	26	1.000±0.014	1.000±0.010	1.000±0.022	1.000±0.012	1.000±0.012	1.000±0.013
Stainless	--	0.990±0.014	0.967±0.011	1.001±0.018	1.001±0.017	1.008±0.011	0.992±0.013
Aluminum	13	0.924±0.012	0.985±0.010	0.966±0.018	0.993±0.012	0.982±0.011	0.970±0.013

Table XX. TLD Analyzer Output Normalized to Iron Encased 1x1x6 mm CaF_2:Mn TLD's Corrected for Individual Sensitivity

Sleeve Material	Z	Normalized Sensitivity Corrected TLD Readout (nc) ± $\sigma_{\bar{x}}$					
		Gamma-ray Energy (MeV)					
		0.136 (11%) 0.122 (87%)	0.145	0.279	0.393	0.662	1.173 (100%) 1.333 (100%)
Lead	82	0.408±0.005	0.521±0.008	1.255±0.010	1.508±0.011	1.450±0.011	1.376±0.014
Tantalum	73	0.488±0.006	0.658±0.010	1.193±0.011	1.399±0.014	1.309±0.012	1.297±0.016
Tin	50	0.995±0.009	1.086±0.018	1.095±0.007	1.142±0.016	1.065±0.012	1.127±0.013
Zirconium	40	1.000±0.007	1.300±0.007	1.015±0.008	1.084±0.009	1.065±0.011	1.051±0.010
Copper	29	0.974±0.006	0.949±0.007	0.981±0.008	0.998±0.009	0.983±0.014	1.068±0.011
Iron	26	1.000±0.008	1.000±0.005	1.000±0.006	1.000±0.007	1.000±0.009	1.000±0.012
Stainless	--	1.001±0.010	0.994±0.004	0.978±0.007	1.006±0.009	1.008±0.010	1.002±0.011
Aluminum	13	1.020±0.008	1.488±0.009	1.009±0.013	1.192±0.011	0.999±0.013	1.001±0.010

Table XXI. Comparisons of Dose Ratios Using Encased ^{7}LiF TLD's from a Precision Subset But Not Corrected for Sensitivity

Sleeve Material	Z	Wall Thickness (g/cm^2)	(C/E) ± $\sigma_{\bar{x}}$ Gamma-ray Energy (MeV) 0.136 (11%) 0.122 (87%)	0.145	0.279	0.393	0.662	1.173 (100%) 1.133 (100%)
Lead	82	0.734	5.245±0.102	5.408±0.085	1.467±0.017	1.110±0.017	0.975±0.018	1.020±0.015
Tantalum	73	0.696	4.618±0.137	3.963±0.138	1.314±0.021	1.066±0.015	0.998±0.017	1.019±0.019
Tin	50	0.608	1.561±0.019	1.333±0.023	1.058±0.013	0.987±0.010	1.037±0.014	1.004±0.018
Zirconium	40	0.514	1.120±0.014	1.059±0.013	1.027±0.016	0.984±0.015	0.995±0.012	0.996±0.011
Copper	29	0.694	1.111±0.023	1.042±0.015	0.990±0.014	1.028±0.013	1.037±0.010	1.017±0.012
Iron	26	0.656	1.000±0.010	1.000±0.015	1.000±0.014	1.000±0.009	1.000±0.013	1.000±0.013
Stainless	--	0.693	1.006±0.014	1.029±0.017	0.994±0.012	0.999±0.012	0.999±0.015	1.014±0.015
Aluminum	13	0.514	0.800±0.011	0.866±0.013	0.976±0.019	0.978±0.012	0.992±0.014	0.991±0.015

Table XXII. Comparison of Dose Ratios Using Encapsulated CaF_2:Mn TLD's from a Precision Subset But Not Corrected for Sensitivity

Sleeve Material	Z	Wall Thickness (g/cm^2)	(C/E) ± $\sigma_{\bar{x}}$ Gamma-ray Energy (MeV) 0.136 (11%) 0.122 (87%)	0.145	0.279	0.393	0.662	1.173 (100%) 1.133 (100%)
Lead	82	0.734	4.128±0.080	3.661±0.059	1.571±0.023	1.093±0.017	1.007±0.014	0.968±0.013
Tantalum	73	0.696	3.251±0.124	2.648±0.048	1.438±0.025	1.038±0.022	1.005±0.011	0.947±0.018
Tin	50	0.608	1.282±0.020	1.186±0.015	1.146±0.014	0.989±0.018	1.022±0.015	0.953±0.014
Zirconium	40	0.514	1.143±0.021	1.150±0.025	1.111±0.017	0.979±0.017	0.983±0.013	0.993±0.017
Copper	29	0.694	1.056±0.018	1.077±0.010	1.036±0.015	1.009±0.015	1.024±0.011	0.944±0.015
Iron	26	0.656	1.000±0.018	1.000±0.009	1.000±0.015	1.000±0.017	1.000±0.013	1.000±0.016
Stainless	--	0.693	0.997±0.015	1.005±0.012	1.018±0.014	0.995±0.014	0.994±0.012	1.004±0.014
Aluminum	13	0.514	0.842±0.012	0.911±0.016	0.969±0.012	0.821±0.013	0.976±0.011	0.968±0.015

Table XXIII. Comparisons of Dose Ratios Using Encased ^{7}LiF TLD's Where the E Values Were Corrected for the Sensitivity of Individual TLD's

Sleeve Material	Z	Wall Thickness (g/cm^2)	(C/E) ± $\sigma_{\bar{x}}$ Gamma-ray Energy (MeV) 0.136 (11%) 0.122 (87%)	0.145	0.279	0.393	0.662	1.173 (100%) 1.133 (100%)
Lead	82	0.734	5.273±0.093	5.453±0.090	1.483±0.026	1.126±0.014	0.981±0.012	1.033±0.014
Tantalum	73	0.696	4.606±0.067	4.000±0.105	1.326±0.024	1.075±0.016	1.001±0.014	1.030±0.012
Tin	50	0.608	1.561±0.024	1.334±0.017	1.065±0.018	0.994±0.010	1.039±0.014	1.012±0.015
Zirconium	40	0.514	1.117±0.013	1.055±0.012	1.032±0.021	0.982±0.012	0.991±0.011	1.000±0.014
Copper	29	0.694	1.085±0.015	1.045±0.012	0.995±0.017	1.020±0.010	1.037±0.014	1.023±0.014
Iron	26	0.656	1.000±0.014	1.000±0.010	1.000±0.022	1.000±0.012	1.000±0.012	1.000±0.013
Stainless	--	0.693	1.008±0.015	1.033±0.012	0.999±0.018	1.001±0.017	0.996±0.011	1.016±0.014
Aluminum	13	0.514	0.798±0.010	0.868±0.009	0.980±0.018	0.982±0.012	0.991±0.011	0.996±0.014

Table XXIV. Comparison of Dose Ratios Using Encased CaF_2:Mn TLD's Where the E Values Were Corrected for the Sensitivity of Individual TLD's.

Sleeve Material	Z	Wall Thickness (g/cm^2)	(C/E) ± $\sigma_{\bar{x}}$ Gamma-ray Energy (MeV)					
			0.136 (11%) 0.122 (87%)	0.145	0.279	0.393	0.662	1.173 (100%) 1.133 (100%)
Lead	82	0.734	4.054±0.048	3.671±0.056	1.579±0.013	1.105±0.008	1.017±0.008	0.970±0.010
Tantalum	73	0.696	3.281±0.039	2.655±0.042	1.452±0.013	1.047±0.010	1.013±0.009	0.954±0.012
Tin	50	0.608	1.287±0.011	1.188±0.020	1.155±0.007	0.995±0.014	1.030±0.011	0.958±0.011
Zirconium	40	0.514	1.138±0.008	1.105±0.007	1.113±0.009	0.977±0.008	0.980±0.010	0.990±0.010
Copper	29	0.694	1.059±0.007	1.081±0.008	1.043±0.008	1.012±0.010	1.027±0.016	0.948±0.010
Iron	26	0.656	1.000±0.008	1.000±0.005	1.000±0.006	1.000±0.007	1.000±0.009	1.000±0.012
Stainless	--	0.693	0.998±0.010	1.005±0.004	1.023±0.007	0.996±0.009	0.995±0.010	1.005±0.010
Aluminum	13	0.514	0.844±0.007	0.912±0.004	0.947±0.012	0.823±0.008	0.979±0.013	0.970±0.010